



## RESEARCH ARTICLE

10.1029/2019JB019028

## Static Source Properties of Slow and Fast Earthquakes

Priyamvada Nanjundiah<sup>1,2</sup> , Sylvain Barbot<sup>3</sup> , and Shengji Wei<sup>1,2</sup> 

<sup>1</sup>Earth Observatory of Singapore, Nanyang Technological University, Singapore, <sup>2</sup>Asian School of the Environment, Nanyang Technological University, Singapore, <sup>3</sup>Department of Earth Sciences, University of Southern California, Los Angeles, CA, USA

## Key Points:

- We compile finite slip distributions for slow and fast earthquakes to quantify static source properties
- The potency density varies systematically with rupture style, tectonic setting, and centroid depth
- The moment-duration scaling of slow-slip events is affected by large variability in potency density

## Supporting Information:

- Supporting Information S1

## Correspondence to:

P. Nanjundiah,  
priyamvada.n@gmail.com

## Citation:

Nanjundiah, P., Barbot, S., & Wei, S. (2020). Static source properties of slow and fast earthquakes. *Journal of Geophysical Research: Solid Earth*, 125, e2019JB019028. <https://doi.org/10.1029/2019JB019028>

Received 9 NOV 2019

Accepted 2 AUG 2020

Accepted article online 10 OCT 2020

**Abstract** The source characteristics of slow and fast earthquakes provide a window into the mechanical properties of faults. In particular, the average stress drop controls the evolution of friction, fault slip, and event magnitude. However, this important source property is typically inferred from the analysis of seismic waves and is subject to many epistemic uncertainties. Here, we investigate the source properties of 53 earthquakes and 17 slow-slip events on thrust and strike-slip faults in various tectonic settings using slip distributions constrained by geodesy in combination with other data. We determine the width, potency, and potency density of slow and fast earthquake sources based on static slip distributions. The potency density, defined conceptually as the ratio of average slip to rupture radius, is a measure of anelastic deformation with limited bias from rigidity differences across depths and tectonic settings. Strike-slip earthquakes have the highest potency density, varying from 20 to 500 microstrain. The potency density is on average lower on continental thrust faults and megathrusts, from 10 to 200 microstrain, with an algebraic decrease with centroid depth, indicative of systematic changes in dominant rupture processes with depth. Slow slip events represent an end-member style of rupture with low potency density and large rupture width. Significant variability in potency density of slow-slip events affects their moment-duration scaling. The variations of source properties across tectonic settings, depth, and rupture styles can be used to better constrain numerical simulations of seismicity and to assess the source characteristics of future earthquakes and slow slip events.

**Plain Language Summary** Natural earthquakes reduce the stress that accumulates on faults due to plate tectonics. To better understand the variability of seismic hazards around active faults, we survey the properties of slow and fast earthquakes around the world. The potential of faults to concentrate large slip in the rupture area differs depending on the geological setting, the depth of the source, and the type of rupture. Earthquakes in a continental setting condense more slip in a given rupture area, particularly in transform faults like the San Andreas fault. Subduction zone earthquakes, although some of the largest events on Earth, generally distribute less slip over a wider area, but this varies as a function of depth. Slow earthquakes represent an extreme case of little slip distributed over a large area. The propensity of rupture characteristics to vary with fault type and depth may help forecast the hazards posed by future seismicity.

## 1. Introduction

The earthquake phenomenon includes a wide spectrum of rupture styles associated with different source characteristics (Beroza & Ide, 2011; Barbot, 2019b; Leeman et al., 2016; Scuderi et al., 2017; Obara & Kato, 2016; Veedu & Barbot, 2016). The stress change on a fault produced by an earthquake is one of the fundamental physical properties that govern the seismic cycle, impacting the style of rupture, that is, slow or fast earthquake, and the magnitude of the event (Aki, 1967, 1979; Barbot et al., 2020; Kanamori & Anderson, 1975; Kanamori et al., 1993; Poli & Prieto, 2016; Sobolev et al., 2017; Venkataraman & Kanamori, 2004; Ye et al., 2016a). The scaling relationship between stress drop and various other source parameters depends on the tectonic setting (e.g., Romanowicz, 1992; Scholz et al., 1986; Walsh & Watterson, 1988) and on the rupture style (Beeler et al., 2001; Cocco et al., 2016; Cattania & Segall, 2018; Gomberg et al., 2016; Kato, 2012; Liu-Zeng et al., 2005; Peng & Gomberg, 2010). Current estimates of stress drop for fast earthquakes typically rely on seismological data, whereby the corner frequency of the source moment-rate function provides rupture duration (e.g., Allmann & Shearer, 2009; Courboux et al., 2016; Shearer et al., 2006; Vallée, 2013;

©2020. The Authors.

This is an open access article under the terms of the Creative Commons Attribution-NonCommercial-NoDerivs License, which permits use and distribution in any medium, provided the original work is properly cited, the use is non-commercial and no modifications or adaptations are made.

Ye et al., 2016b) and a theoretical model is used to estimate an effective rupture length (Brune, 1970; Kaneko & Shearer, 2014; Madariaga, 1976, 1977). However, stress drop estimates based on seismological approaches are subject to large uncertainties (Baltay et al., 2011; Prieto et al., 2006), for example, due to trade-offs between rupture velocity and rise time, the amplitude of high-frequency waves and attenuation (Baltay & Hanks, 2014), and between the rupture velocity and the overall slip area. Additional bias, especially for large events, may also arise from overly simplifying assumptions about the rupture process including directivity, single versus multi-pulse ruptures, geometry (Kaneko & Shearer, 2015), estimation of the overall duration of the event (Courboulex et al., 2016) and unknown variations in elastic properties of the surrounding rocks.

To mitigate these issues, we consider finite slip distributions of slow and fast earthquakes constrained by geodetic data, along with other measurements. Inversion of geodetic data for the spatial distribution of slip on a fault is also subject to fundamental limitations, notably due to the St. Venant principle that implies a decreasing resolution with increasing distance between source and observations. However, the deployment of increasingly large and dense geodetic observatories, the development of better analytic standards in inverse theory (Aster et al., 2012; Funning et al., 2014; Fukahata & Wright, 2008; Hang et al., 2020; Nocquet, 2018; Yabuki & Matsu'ura, 1992), and the joint inversion of complementary data sets, both geodetic and seismological, has increased the accuracy of slip distributions (Atzori & Antonioli, 2011; Amey et al., 2018; Barbot et al., 2013; Duputel et al., 2014; DeVries et al., 2017; Evans & Meade, 2012; Gombert et al., 2017, 2018; McGuire & Segall, 2003; Minson et al., 2014; Sathiakumar et al., 2017). For example, the large uncertainties associated with shallow slip near the trench during the 2011 Mw = 9.1 Tohoku, Japan, earthquake were largely reduced by considering tsunami data (e.g., Bletery et al., 2014; Jiang & Simons, 2016; Yamazaki et al., 2011). Rupture of subduction megathrusts can also be well imaged by combining high-rate Global Positioning System (GPS), teleseismic body waves, synthetic aperture radar interferometry (InSAR), campaign GPS, and tsunami observations (Yue et al., 2014). The slip distribution of continental earthquakes is increasingly well resolved by space geodetic observations, notably as InSAR can constrain the three-dimensional surface displacement with high spatial resolution (Avouac et al., 2015; Bechor & Zebker, 2006; Barbot et al., 2008; Fialko et al., 2001, 2005; Fialko, 2004; Moore et al., 2017; Wang & Jónsson, 2015; Wang, Wei, et al. 2018; Wang, Shi, et al. 2018; Wang, Zhang, et al. 2018).

Geodetic-based slip distributions of slow and fast earthquakes may constrain the geometric properties of ruptures, that is, the effective length, width, and area (e.g., Brengman et al., 2019; Weston et al., 2012), but a remaining issue regarding stress drop is large variations of elastic properties across tectonic settings and source depths. The variability of elastic properties should be accounted for to compare estimates of stress drop for events in different tectonic settings or depth, but the elastic properties are not always well known. Following the previous suggestion of quantifying the size of earthquakes with the seismic potency  $P = As$  instead of the seismic moment  $M = GAs$  (Ben-Zion, 2001; Ben-Zion & Zhu, 2002), where  $G$  is the rigidity,  $A$  is the rupture area, and  $s$  is the representative fault slip, we propose to look at the average potency density of the rupture. We define potency density as an extrinsic (external) property of ruptures that represents a characteristic strain, defined as the ratio of fault slip to rupture length

$$\epsilon = c \frac{s}{R}, \quad (1)$$

where  $R$  is a characteristic length scale such that  $A = R^2$  and  $c \sim 1$  is a non-dimensional constant controlled by geometry. That strain corresponds to a potency density becomes evident when considering the relationship with seismic potency, that is,  $P \propto \epsilon R^3$  or  $\epsilon \propto P/R^3$ . Our definition therefore differs from that of Ben-Zion et al. (2003) and Ben-Zion and Lyakhovsky (2019) that refer to the local potency per unit volume as an intrinsic property. As a suitable alternative to the potency density defined in Equation 1, Vallée (2013) uses the term strain drop to refer to the same quantity, but the name may be ambiguous because as elastic strain indeed decreases around a rupture, anelastic strain in fact accrues.

A dimensional analysis shows that the recurrence time of instabilities is controlled by potency density, as in  $T_r \propto \epsilon R/V_L$ , where  $V_L$  is the fault long-term loading rate. The potency density is also related to the static stress drop, following

$$\Delta\tau = 2G\epsilon, \quad (2)$$

where the factor of 2 comes from Hooke's law in three dimensions. Hence, the potency density provides a useful source property relevant to both slow and fast earthquakes that can be estimated from static slip distributions with limited bias from unknown variations in elastic properties.

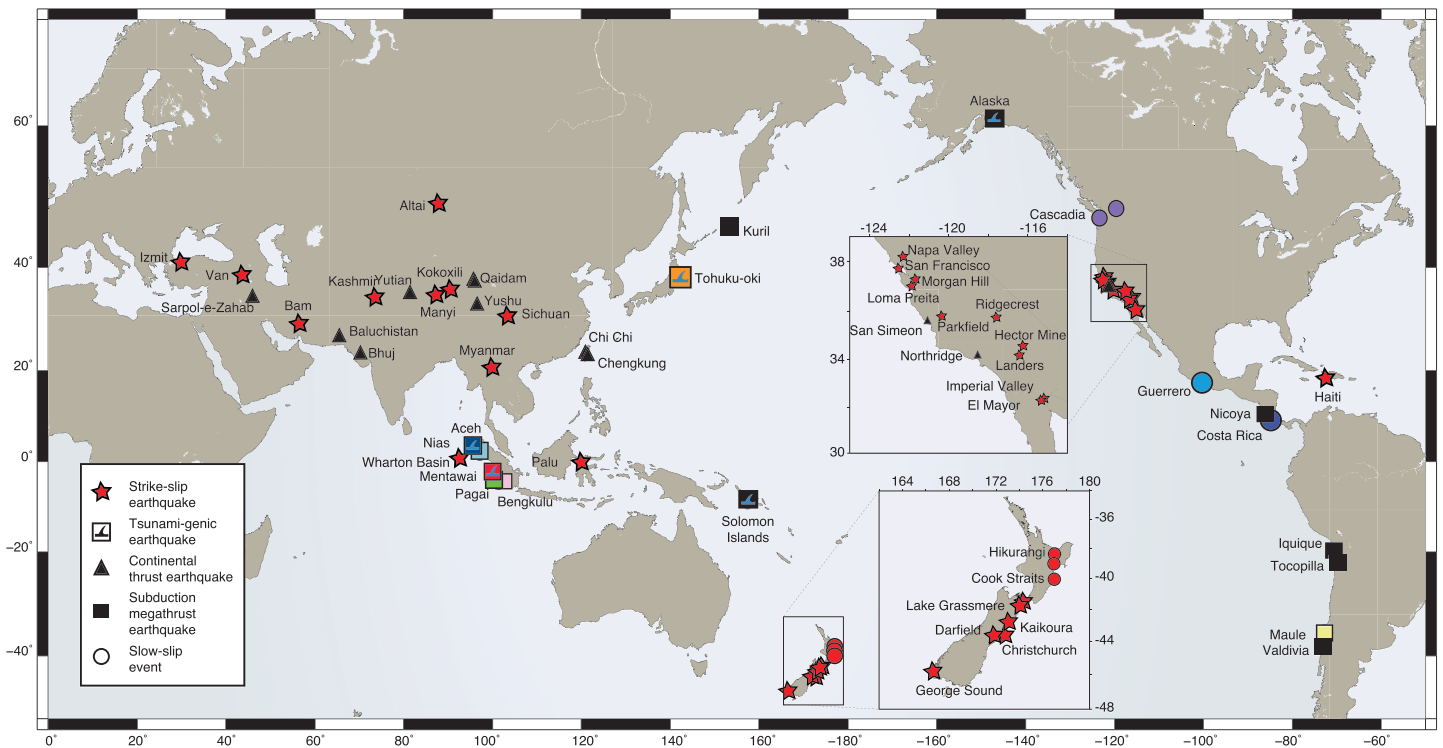


**Figure 1.** The distribution of slow and fast earthquakes considered in this study. The catalog includes thrust fault and megathrust earthquakes (25 events), strike-slip fault earthquakes (red stars, 28 events), and slow-slip events on subduction megathrusts (circles, 17 events), adding to 70 events. The squares represent megathrust events; the color is for rapid identification in subsequent figures. The triangles show continental thrust earthquakes.

In this study, we build a curated catalog of slip distributions based on the analysis of geodetic and other geophysical data for thrust-fault and megathrust earthquakes (25 events), strike-slip fault earthquakes (28 events), and slow-slip events on subduction megathrusts (17 events), adding to 70 events (Figure 1). The slip distributions are obtained from a long legacy of published work (67 events) and original results (three events) for the 2015 Mw 7.2 Lake Sarez (Tajikistan), 2018 Palu (Indonesia), and 2019 Ridgecrest (California) earthquakes. Unfortunately, not enough data are available to characterize normal faulting events. In section 2, we describe the methodology to derive the width, potency, and potency density automatically from the finite slip distributions. In section 3, we present the catalog and the relationships among source characteristics. We find that the down-dip rupture extent of slow and fast earthquakes increases with centroid depth. Notably, the potency density of subduction earthquakes seems to decrease with depth, indicating that different rupture processes operate at different depths. We also discuss the impact of potency density on the moment-duration scaling relationship of slow-slip events.

## 2. Static Source Properties From Finite Slip Distributions

We seek a systematic approach to analyze a large number of slip distributions that have in common a complex source geometry, including non-uniform slip distribution, several branches of varying strike and dip, and rake variations. For a circular patch of radius  $R$  with uniform slip  $s$ , the potency density finds a closed-form expression (Eshelby, 1957)

$$\epsilon = \frac{7\pi s}{32 R}. \quad (3)$$

Some authors (e.g., Barbot et al., 2009; Brown et al., 2015; Somerville et al., 1999) estimate the effective radius and the mean slip in finite slip distributions to approximate the potency or the stress drop using Equations 2 and 3. Mai and Beroza (2000) first estimate rupture dimensions and then estimate an average slip that conserves the total seismic moment. These approaches are problematic in our case because they either rely on arbitrary slip thresholds to define the slip area, ignore the geometrical intricacies of ruptures, or cannot address the issues associated with multiple fault strands. A single slip threshold is not applicable to treat a catalog of events with magnitudes range from  $M_w = 6.0$  to  $M_w = 9.5$ .

We propose an estimate of the potency density that can be applied to realistic slip distributions with multiple fault strands, rake rotations, and possibly non-planar faults. Consider a fault surface  $\partial\Omega$  with varying normal vector  $\hat{\mathbf{n}}$  associated with a slip distribution  $\mathbf{s}$ . The deformation of the surrounding rocks leads to a distribution of strain  $\epsilon$  in the elastic medium. Strain is a symmetric, second-order tensor. To reduce the tensor field to a scalar quantity, we seek an average of the strain components aligned with the shear dislocation defined by the dyadic product  $\hat{\mathbf{n}} \otimes \hat{\mathbf{s}}$  along the fault (Barbot & Fialko, 2010), where the hat indicates a unit vector, such that  $\mathbf{s} = s\hat{\mathbf{s}}$ , with  $s \geq 0$ . Following the estimates of stress drop based on energy considerations proposed by Noda et al. (2013), we use a weighted average of the strain components based on slip,

$$\epsilon = - \frac{\int_{\partial\Omega} \epsilon : (\hat{\mathbf{n}} \otimes \mathbf{s}) dA}{\int_{\partial\Omega} s dA}, \quad (4)$$

where the symbol  $:$  is the double-dot product (Nemat-Nasser & Hori, 1996; Nemat-Nasser, 2004). The estimate of potency density in Equation 4 can be obtained without imposing any arbitrary thresholds on rupture area or slip and is applicable to any slip distribution regardless of complexity. The formulation also accounts for rake rotations and is independent of rigidity. Since slip is used as a weighting factor, the fault area devoid of slip is naturally excluded. This process is illustrated in Figure 2 using the slip distribution of the 2015 Mw 7.2 Lake Sarez earthquake, which was obtained by inversion of SAR data. The slip distribution features varying strike, dip, and rake along the rupture (Figure 2a). The strain distribution on the fault plane, computed as  $\epsilon : (\hat{\mathbf{n}} \otimes \hat{\mathbf{s}})$ , is shown in Figure 2b. Most areas of positive strain change are associated with regions of little to no slip and are weighted out. Meanwhile, the areas of smooth slip distribution that would be difficult to outline with a slip threshold, for example, to the southwest, are associated with little strain, contributing minimally to the overall potency density estimation. The method can then be applied uniformly to events of various sizes. When treating the entire catalog of events, we consider finite slip distributions with fault surfaces decomposed into rectangular or triangular meshes. We calculate the strain tensor at the patch centers assuming a uniform half-space with Poisson's ratio  $\nu = 0.25$  using the analytical solution of Okada (1992) for rectangular dislocations and the one of Nikkhoo and Walter (2015) for triangular dislocations. If the elastic properties are uniform, the deformation does not depend on the rigidity. When calculating potency density, we ignore vertical or lateral variations of elastic moduli.

In the same vein, we seek to describe the geometrical properties of ruptures from finite slip distributions without potential bias from arbitrary thresholds for slip, such that slow and fast, small and large earthquakes can be treated consistently. The definition of rupture width can vary depending on the data considered. Rupture length can be estimated from surface slip (Manighetti et al., 2001, 2007; Wyss, 1979), or from the spatial extent of early aftershocks (Kanamori & Anderson, 1975; Robert & Darragh, 1987), leading to different results (Wells & Coppersmith, 1994). We use slip as a weighting factor and estimate the centroid location as follows:

$$\bar{z} = \frac{\int_{\partial\Omega} z s dA}{\int_{\partial\Omega} s dA}, \quad (5)$$

where  $\bar{z}$  is the centroid depth and  $z$  is the depth of the fault surface. To facilitate the comparison of ruptures occurring on faults with different dip angles, we focus on the depth extent of ruptures instead of the down-dip rupture width. On quasi-vertical strike-slip faults, comparing the depth extent or the down-dip extent is equivalent. On gently dipping faults, considering the depth extent is useful to understand the potential relationship between rupture geometry and stratigraphy or the overall vertical thermo-mechanical structure of the plate boundary. To estimate the rupture width in the depth direction, we treat rupture depth as a random variable. We do not make any specific assumption about the probability density distribution of depth, except for the fact that it is a positive quantity, and therefore, a Gaussian distribution is not appropriate, unavoidably predicting non-zero probability of negative depths (Tarantola, 2004). To avoid this issue, we manipulate the logarithm of depth. For example, if the logarithm of depth was normally distributed, then depth would be log-normally distributed, predicting zero probability of slip above the surface. Accordingly, we first compute another estimate of the centroid depth as

$$\begin{aligned} \bar{w} &= \log_{10}(\bar{z}^*) \\ &= \frac{\int_{\partial\Omega} \log_{10}(z) s dA}{\int_{\partial\Omega} s dA}, \end{aligned} \quad (6)$$

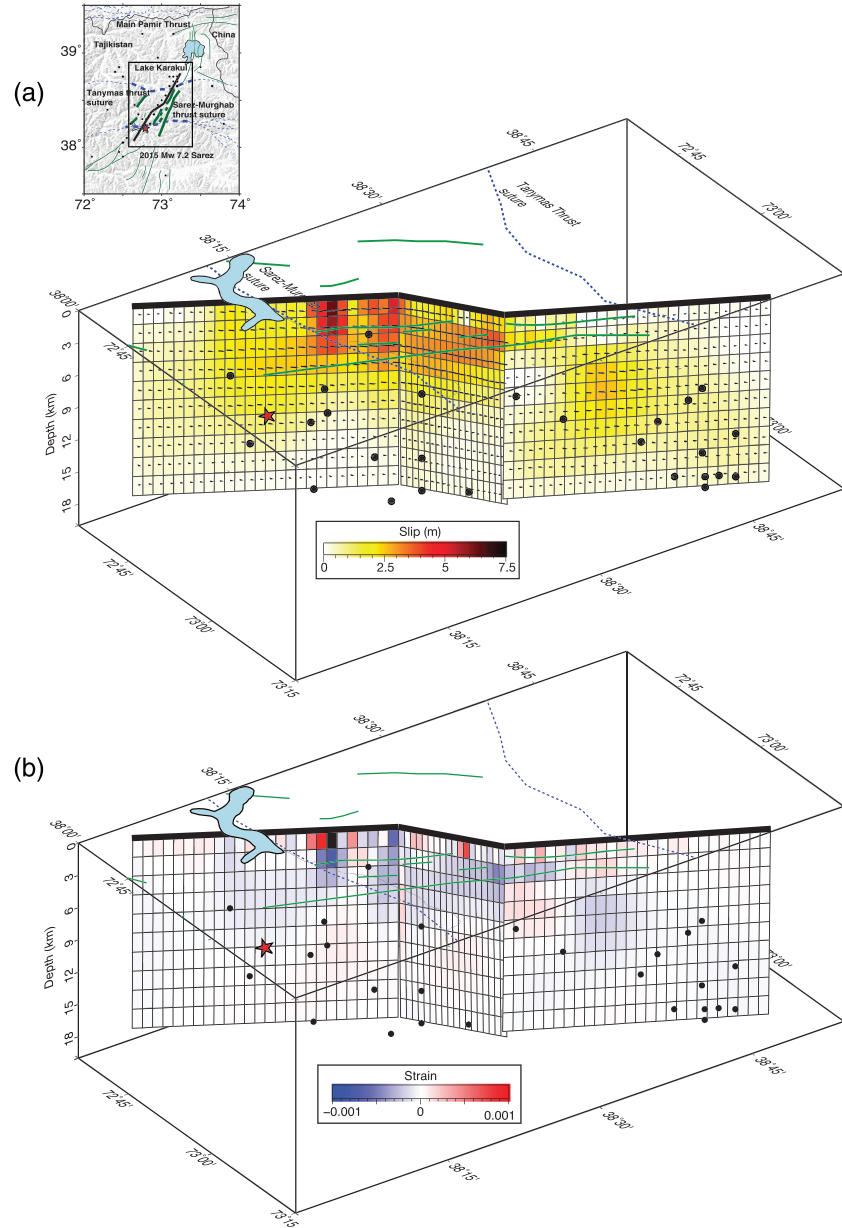


**Figure 2.** Slip and strain distribution for the 2015 Mw 7.2 Lake Sarez, Tajikistan earthquake. a) Slip distribution inferred from SAR and InSAR data. The star marks the hypocenter. b) Distribution of strain along the fault. When averaged over the entire slip region and weighted by slip, the potency density of the earthquake is estimated at 96.1 microstrain.

where  $\log_{10}(x) = \log(x)/\log(10)$ . We then estimate the standard deviation of the depth distribution

$$\bar{\sigma}^2 = \frac{\int_{\partial\Omega} [\log_{10}(z) - \bar{w}]^2 s dA}{\int_{\partial\Omega} s dA}. \quad (7)$$

Finally, we define the rupture width in the depth direction as the range of depths that would encompass more than 98% of the slip distribution if depth was log-normally distributed, that is,  $W = 10^{w+\bar{\sigma}} - 10^{w-\bar{\sigma}}$ . Simplifying this expression, we obtain

$$W = 2\bar{z}^* \sinh(\sigma \log(10)). \quad (8)$$

**Table 1**

*Slip Distribution and Source Characteristics of 28 Strike-Slip Fault Earthquakes From Magnitude  $M_w = 6.0$  to 8.6 Considering 35 Different Models*

Name	Country/Region	Year	$M_w$	Potency density	Centroid depth (km)	Width (km)	Reference
Altai	Russia	2003	7.2	287.9	7.1	10.2	Barbot et al. (2008)
Balochistan	Pakistan	2013	7.7	63.2	9.5	13.2	Avouac et al. (2014)
Bam	Iran	2003	6.6	82.28	2.6	4.157	Fialko et al. (2005)
Christchurch	New Zealand	2011	6.3	263.7	6.0	6.2	Elliott et al. (2012)
Cook Straits	New Zealand	2013	6.6	22.1	15.3	11.0	Hamling et al. (2014)
Darfield	New Zealand	2010	6.9	344.7	5.3	7.0	Elliott et al. (2012)
El Mayor	Mexico	2010	7.2	71.6	5.2	5.2	Wei et al. (2013)
Haiti	Haiti	2010	7.0	130.8	12.4	12.4	Symithe et al. (2013)
Hector Mine	USA	1999	7.1	259.1	6.4	8.2	Salichon et al. (2004)
Imperial Valley	USA	1979	6.3	154.7	5.7	5.7	Zeng and Anderson (2000)
Izmit	Turkey	1999	7.6	87.6	8.1	11.7	Toksoz et al. (1999)
Kaikoura	New Zealand	2016	7.9	325.7	15.8	19.0	Wang, Wei, et al. (2018)
Kokoxili	China	2001	7.9	81.8	8.7	11.4	Lasserre et al. (2005)
Kumomoto	Japan	2016	7.3	188.3	10.2	11.1	Moore et al. (2017)
Landers	USA	1992	7.3	263.5	3.4	5.3	Fialko (2004)
Lake Grassmere	New Zealand	2013	6.6	47.0	9.7	11.5	Hamling et al. (2014)
Lake Sarez	Tajikistan	2015	7.2	96.1	6.5	9.1	Nanjundiah, pers. comm.
Loma Prieta	USA	1989	6.9	354.7	12.7	8.0	Zeng and Anderson (2000)
Manyi	China	2004	7.6	76.7	7.1	9.3	Wang et al. (2007)
Morgan Hill	USA	1984	6.3	154.0	9.0	7.1	Beroza and Spudich (1988)
Myanmar	Myanmar	2011	6.9	127.0	4.4	6.1	Wang et al. (2014)
Napa Valley	USA	2014	6.0	30.7	6.7	9.2	Wei et al. (2015)
Palu	Sulawesi	2018	7.5	204.8	7.3	8.14	S. Wei, pers. comm.
Parkfield	USA	2004	6.0	33.1	7.1	7.4	Barbot et al. (2012)
Ridgecrest	USA	2019	7.1	407.3	9.9	12.6	S. Wei, pers. comm.
San Francisco	USA	1906	7.9	98.5	6.0	6.0	Song et al. (2008)
Van	Turkey	2011	7.1	422.2	14.3	8.9	Elliott et al. (2013)
Wharton Basin	Sumatra	2012	8.6	211.1	15.7	33.4	Hill et al. (2015)

These estimates can accommodate non-planar faults, multiple strands, and non-uniform slip distributions. The estimates of rupture dimension and potency density are independent beyond the fact that they use the same slip distribution.

### 3. Source Characteristics of Earthquakes and Slow-Slip Events

We compile a collection of finite slip distributions for slow and fast earthquakes based on the analysis of geodetic and other geophysical data (Figure 1). We curate a catalog based on the data set used to constrain the models, the quality of the inversion procedure, in particular whether an objective criterion is used for the degree of regularization, and the absence of unrealistic features like spurious slip concentration at the boundary of the discretized fault. We collect published slip distributions for 53 earthquakes and 17 slow-slip events and combine them in a uniform format where the slip, position, length, width, strike, dip, and rake is documented for every rectangular patch, and additionally, the vertex coordinates for triangular dislocations. Among the earthquakes, we have 28 strike-slip fault earthquakes and 25 thrust fault and megathrust earthquakes. The catalog includes strike-slip fault earthquakes from moment magnitude  $M_w = 6.0$  to 8.6 and thrust earthquakes from magnitude  $M_w = 6.3$  to 9.2.

All models are constrained by geodetic data, that is, GPS and/or InSAR, but may also include regional and teleseismic data and tsunami records. In some cases, only one model satisfies the requirements and can be found in digital form. However, in many cases, the same event is documented in several studies. Collectively,

**Table 2**

*Slip Distributions and Source Characteristics of 25 Thrust and Megathrust Earthquakes Considering 34 Different Models*

Name	Country/Region	Year	Mw	Potency density	Centroid depth (km)	Width (km)	Reference
Aceh	Sumatra	2004	9.2	34.9	32.2	22.75	Chlieh et al. (2007)
Alaska	USA	1964	9.2	22.0	16.0	12.0	Johnson et al. (1996)
Bengkulu	Sumatra	2007	8.4	9.4	32.13	36.8	Tsang et al. (2016)
Bhuj	India	2001	7.6	182.7	14.5	19.1	Copley et al. (2011)
Chengkung	Taiwan	2003	6.8	9.6	20.2	20	Thomas et al. (2014)
Chi-Chi	Taiwan	1999	7.5	170.7	3.4	4.01	Yu et al. (2001)
Gorkha	Nepal	2015	7.8	22.2	14.5	9.2	Wei et al. (2018)
Iquique	Chile	2014	8.2	20.5	25.5	39.0	Gusman et al. (2015)
Kashmir	Kashmir	2005	7.6	118.4	7.2	9.15	Avouac et al. (2006)
Kuril	Alaska	2006-07	8.3	9.1	9.3	11	Steblov et al. (2008)
Maule	Chile	2010	8.8	36.3	36.8	22.8	Luttrell et al. (2011)
Mentawai	Sumatra	2010	7.8	132.7	6.3	4.7	Yue et al. (2014)
Nias	Sumatra	2005	8.6	40.9	28.3	15.6	Konca et al. (2007)
Nicoya	Costa Rica	2012	7.6	35.5	20.6	22.5	Yue et al. (2013)
Northridge	USA	1994	6.9	113.6	9.7	9.8	Hudnut et al. (1996)
Pagai	Sumatra	2008	7.2	35.5	17.2	5.4	Salman et al. (2017)
Qaidam	China	2008	6.3	139.2	16.5	9.6	Elliott et al. (2011)
Qaidam	China	2009	6.3	198.5	5.6	4.7	Elliott et al. (2011)
San Simeon	USA	2003	6.5	126.7	6.1	5.3	Ji et al. (2004)
Sarpol Zahab	Iran	2017	7.3	128.9	14.6	4.8	Feng et al. (2018)
Solomon Isl.	Solomon Isl.	2010	7.1	110.0	2.4	2.3	Newman, Feng, et al. (2011)
Tohoku-Oki	Japan	2011	9.1	160.8	6.9	17.7	Bletery et al. (2014)
Tocopilla	Chile	2007	7.7	12.0	36.1	16.6	Bejar Pizarro et al. (2010)
Valdivia	Chile	1960	9.6	93.7	24.0	19.0	Moreno et al. (2009)
Yushu	China	2010	6.9	43.9	6.8	9.9	Li et al. (2011)

the 70 events considered here are documented in at least 109 different models. For example, several sophisticated models of the 1992 Mw = 7.3 Landers, California, earthquake based on seismic and geodetic data can be found (e.g., Hernandez et al., 1999; Wald & Heaton, 1994), but we prefer the model of Fialko (2004) based on a reconstruction of the three-dimensional surface displacements at high spatial resolution. The surface displacements of the 2010 Mw = 7.2 El Mayor-Cucapah earthquake was constrained by InSAR data (Wei et al., 2011), but the model of Wei et al. (2013) includes teleseismic and regional seismic data, improving resolution at depth. Similarly, the 1999 Mw = 7.1 Hector Mine earthquake was constrained with geodesy (Simons, 2002), but the model of Salichon et al. (2004) includes InSAR, GPS, and teleseismic data. Model selection has an important impact on the estimation of potency density. For the Hector Mine earthquake, the models of Simons (2002) and Salichon et al. (2004) imply a potency density of 168 and 259 microstrain, respectively. For the Parkfield earthquake, the models of Ji et al. (2004), Dreger et al. (2005), and Barbot et al. (2012) imply potency densities of 45, 22, and 33 microstrain, respectively. This indicates that the epistemic uncertainties associated with model discretization, data selection, and inversion methods are multiplicative. The variability found in multiple models of the same event indicates that the potency density is well constrained within a factor of two. Although these estimates may vary significantly within that range, these differences pale in regard to the overall variability of potency density across strike-slip fault earthquakes, from 20 to 500 microstrain, covering about 2 orders of magnitude. Among strike-slip fault earthquakes, we find that model selection has no impact on the relationships among source characteristics, as there is no systematic variation of potency density with depth or magnitude for this type of event.

The source properties of subduction megathrust earthquakes are more sensitive to model selection due to the various assumptions affecting shallow slip near the trench (e.g., Loveless & Meade, 2011). In particular, a prevailing but incorrect assumption has been that fault slip in the accretionary region is aseismic. However, accretionary prisms are known to produce tsunami earthquakes (Bilek & Lay, 2002; Geersen, 2019;

**Table 3**

*Slip Distributions and Source Characteristics of 17 Slow-Slip Events on Subduction Megathrusts Used in the Study*

Name	Country	Year of event	Magnitude	Potency density	Centroid depth	Width	Duration (days)	Reference
Cascadia	USA/Canada	2008	6.75	0.103	35.8	12.5	38	Dragert and Wang (2011)
Cascadia	USA/Canada	2010	6.84	0.029	36.4	29.92	58	Goodner (2014)
Cascadia	USA/Canada	2011	6.77	0.03	36.61	32.32	56	Goodner (2014)
Cascadia	USA/Canada	2012	6.83	0.018	35.86	36.25	51	Goodner (2014)
Cascadia	USA/Canada	2013	6.85	0.035	38.19	34.08	NA	Goodner (2014)
Costa Rica	Costa Rica	2007	6.92	1.811	45.8	36.86	63	Dixon et al. (2014)
Costa Rica	Costa Rica	2008	6.48	0.141	37.62	34.15	20	Dixon et al. (2014)
Costa Rica	Costa Rica	2009	6.97	2.933	44.6	36.03	180	Dixon et al. (2014)
Costa Rica	Costa Rica	2010	6.46	0.792	37.6	31.37	30	Dixon et al. (2014)
Costa Rica	Costa Rica	2011	6.61	0.377	27.02	23.7	20	Dixon et al. (2014)
Costa Rica	Costa Rica	2012	6.94	1.282	32.78	35.51	112	Dixon et al. (2014)
Guerrero	Mexico	2002	7.65	0.299	34.48	22.9	122	Radiguet (2012)
Guerrero	Mexico	2006	7.49	0.359	34.5	20.7	180	Radiguet (2012)
Guerrero	Mexico	2010	7.53	0.648	33.8	13.51	180	Radiguet (2012); Bekaert et al. (2015)
Hikurangi	New Zealand	2006	6.55	0.43	38.5	30.41	122	Wallace and Eberhart-Phillips (2013)
Hikurangi	New Zealand	2008	6.58	0.372	33.9	20.93	91	Wallace and Eberhart-Phillips (2013)
Hikurangi	New Zealand	2013	6.95	1.17	9.9	3.51	12	Wallace and Eberhart-Phillips (2013)

Kanamori, 1972; Pelayo & Wiens, 1992; Satake & Tanioka, 1999), the rupture of giant earthquakes often reaches the trench (e.g., Fujiwara et al., 2011; Ishii et al., 2005; Lorenzo-Martín et al., 2006; Tomita et al., 2017; Yue et al., 2014), and low-frequency earthquakes and tectonic tremors occur at shallow depth at subduction zones (Dixon et al., 2014; Jiang et al., 2012; Nakano et al., 2018; Toh et al., 2018; Wallace et al., 2016, 2017). Among the slip distributions of giant earthquakes, that is, the 2004 Mw = 9.2 Sumatra-Andaman (Indonesia), 2011 Mw = 9.1 Tohoku-Oki (Japan), and 2010 Mw = 8.8 Maule (Chile) earthquakes (Chlieh et al., 2007; Inuma et al., 2012; Lorito et al., 2011; Luttrell et al., 2011; Rhie et al., 2007; Simons et al., 2012; Wei et al., 2012) and tsunami earthquakes (Bilek et al., 2011; Newman, Hayes, et al. 2011; Satake et al., 2013; Yue et al., 2014), we select those that mitigate uncertainty in shallow slip by incorporating geodetic measurements with tsunami and other geophysical data. Even with these restrictions, the epistemic uncertainties associated with meshing, regularization, and data selection introduce large variability in source characteristics. For example, the models of Wei et al. (2012), Yamazaki et al. (2011), and Bletery et al. (2014) for the 2011 Mw = 9.1 Tohoku-Oki earthquake imply a potency density of 51, 102, and 160 microstrain, respectively, and a centroid depth of 18, 14, and 7 km, respectively. These source characteristics are also well constrained within a factor of two. However, given the range of potency density from 10 to 200 microstrain and of centroid depths from 2 to 50 km among thrust earthquakes, these uncertainties do not significantly affect the overall depth dependence of potency density for this type of events.

For each finite slip distribution of slow and fast earthquakes, we estimate the width in the depth direction, potency, and potency density. The supporting information include the slip distributions in a uniform format and the estimated source characteristics for all published models available. When multiple slip models are available, we select the one from the most comprehensive study. The source characteristics are listed in Table 1 for strike-slip earthquakes, Table 2 for thrust and megathrust earthquakes, and Table 3 for megathrust slow-slip events. We cluster the events in groups of broadly similar tectonic settings, including strike-slip faults, thrust faults, and megathrusts. We further identify the tsunamigenic earthquakes, which include any earthquake that generated a substantial tsunami, encompassing the so-called tsunami earthquakes that generate a tsunami larger than what would be anticipated for their magnitude (Kanamori, 1972).

The source characteristics of strike-slip fault earthquakes for the catalog considered are shown in Figures 3a, 4a, and 5. The potency density of strike-slip fault earthquakes varies from 20 to 500 microstrain, the smallest value being associated with the 2013 Mw = 6.6 Cook Strait, New Zealand, earthquake (Hamling et al., 2014), presumably biased due to the depth and offshore location of the slip patch. The largest potency

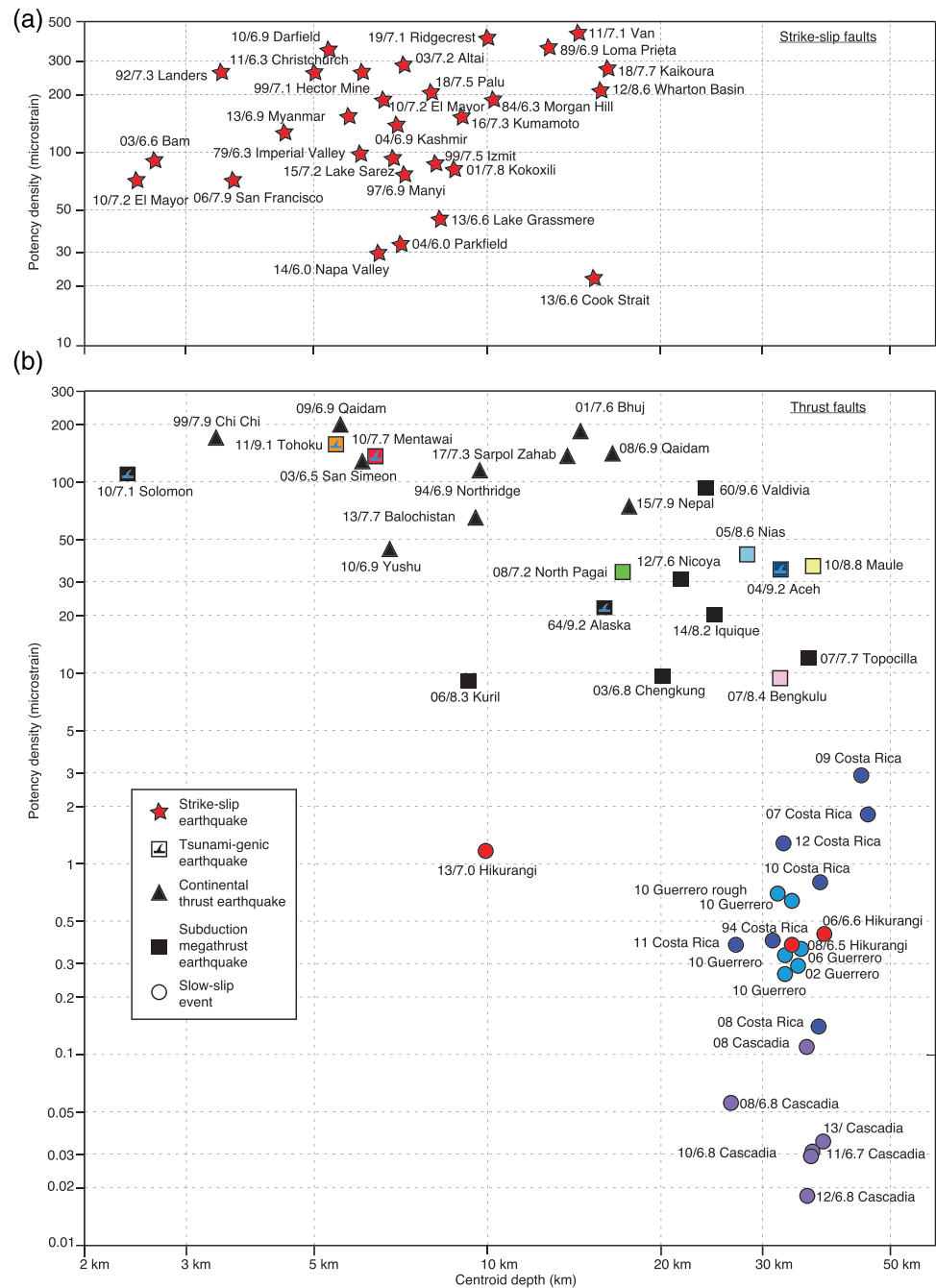


**Figure 3.** Variation of potency density with centroid depth of all events in the catalog. (a) Distribution of potency density with centroid depth for strike-slip earthquakes. (b) Potency density of thrust faults and megathrust events. Shallow events, predominantly strike-slip or tsunami earthquakes, are characterized with large potency density. Deep megathrust earthquakes tend to have a lower potency density. Deep slow-slip events, with potency densities orders of magnitude smaller than strike-slip fault earthquakes, form an end-member of rupture style.

density is found for the 2011  $M_w = 6.3$  Christchurch, New Zealand, the 2011  $M_w = 7.1$  Van, Turkey, and the 2019  $M_w = 7.1$  Ridgecrest earthquakes, illustrating the independence with earthquake magnitude. The 1992  $M_w = 7.3$  Landers, the 1999  $M_w = 7.1$  Hector Mine, and the 2018  $M_w = 7.7$  Kaikoura earthquakes have a similar potency density of  $\sim 260$  microstrain, despite their different centroid depths of 4, 5, and 16 km depth, respectively. Overall, we find that strike-slip fault earthquakes have the largest potency density among all events in the catalog, with no systematic trend among source characteristics, except for an increase in rupture width with centroid depth.





and centroid depth for slow-slip events from Costa Rica (Dixon et al., 2014), Guerrero, Mexico (Bekaret et al., 2015; Radiguet et al., 2012), Hikurangi, New Zealand (Wallace & Eberhart-Phillips, 2013), and Cascadia, Pacific Northwest (Goodner, 2014; Schmidt & Gao, 2010). However, like it seems to apply to all types of events, the depth extent of slow-slip ruptures increases with their centroid depth.

#### 4. Discussion

Our analysis reveals that potency density is independent of rupture size, considering ruptures of the same type and tectonic setting, consistent with seismological studies of stress drop (Allmann & Shearer, 2009; Kanamori & Anderson, 1975; Miyakoshi et al., 2019; Venkataraman & Kanamori, 2004; Ye et al., 2016b). The independence of potency density with size for ruptures of any type is compatible with the idea that stress drop or potency density is a fundamental property of ruptures leading to self-similarity of the earthquake phenomenon (Cocco et al., 2016). Vallée (2013) shows that global earthquakes from the surface to 600 km depth are compatible with a constant strain drop model, although his data for events shallower than 50 km show significant scatter. Analysis of shallow earthquakes based on the same technique (Courboulex et al., 2016) shows no particular trend between stress drop and magnitude, but the changes with depth or tectonic setting are not discussed.

Our analysis shows systematic differences of potency density among types of ruptures and tectonic settings. Continental strike-slip fault earthquakes on average have the largest potency density, between 20 and 500 microstrain. Continental thrust faults earthquakes have the second highest potency density, between 40 and 200 microstrain. Shallow subduction zone ruptures, including tsunami earthquakes, are characterized with large potency density, between 100 and 200 microstrain. Deep megathrust earthquakes form a group of the lowest overall potency density, between 10 and 100 microstrain. Finally, slow-slip event form a category of their own, with a potency density between 0.01 and 3 microstrain.

The 2010  $M_w = 7.7$  Mentawai tsunami earthquake exhibits a particularly high potency density compared to other megathrust earthquakes, including the tsunamigenic 2008  $M_w = 7.2$  North Pagai earthquake (Salman et al., 2017). The large potency density of tsunami earthquakes may indicate the activation of strong-weakening mechanisms for near-trench ruptures, such as thermal pressurization of the frictional interface proposed by Mitsui et al. (2012) and Noda and Lapusta (2013). The simultaneous high potency density and low stress drop of tsunami earthquakes are compatible due to the low rigidity of surrounding rocks in the accretionary prism (Sallarès & Ranero, 2019).

Deep megathrust earthquakes exhibit a lower potency density and a larger rupture width than any other earthquake category. It is possible that the deep ruptures propagate into nominally slow-slip or velocity-strengthening regions, reducing their average potency density in the process. This may explain why no periodic slow-slip has been found at subduction zones where a deep rupture recently took place, such as at the Japan trench (Agata et al., 2019; Muto et al., 2019) or the Sunda Trench (Hoechner et al., 2011), as the exceedingly large stress reduction caused by a large rupture may have interrupted the slow-slip cycle for a few decades (Feng et al., 2015; Herrendörfer et al., 2015; Shi et al., 2020). The low potency density of deep megathrust ruptures may also be caused by their proximity to the stability transition zone, which may manifest itself by a gradual reduction of coseismic weakening with increasing temperature before stable-weakening or firmly velocity-strengthening properties are attained at greater depths.

The tendency of ruptures to increase width with increasing centroid depth is clear within the catalog (Figure 5), particularly as both rupture width and centroid depth do not scale with seismic potency (Figures 6 and 7). However, this trend may be biased in part by the upper bound of rupture width from the free surface. Indeed, by construction, the effective width cannot exceed twice the centroid depth. It is also likely that considering more events of smaller magnitude may fill the lower right quadrant of Figure 5. Ruptures on different types of faults follow a different scaling with centroid depth. Continental strike-slip events follow  $w = 10^{0.43} z^{0.561}$ , continental thrust earthquakes  $w = 10^{0.4} z^{0.527}$ , shallow megathrust events  $w = 10^{0.03} z^{0.93}$ , and other megathrust events  $w = 10^{0.12} z^{0.86}$ . The sub-linear relationship between width and centroid depth in log-log space for all events, with a power exponent of 0.76, indicates the tendency of most earthquakes to not break the surface, or to exhibit less slip near the surface, broadly compatible with the concept of shallow slip deficit (Fialko et al., 2005).

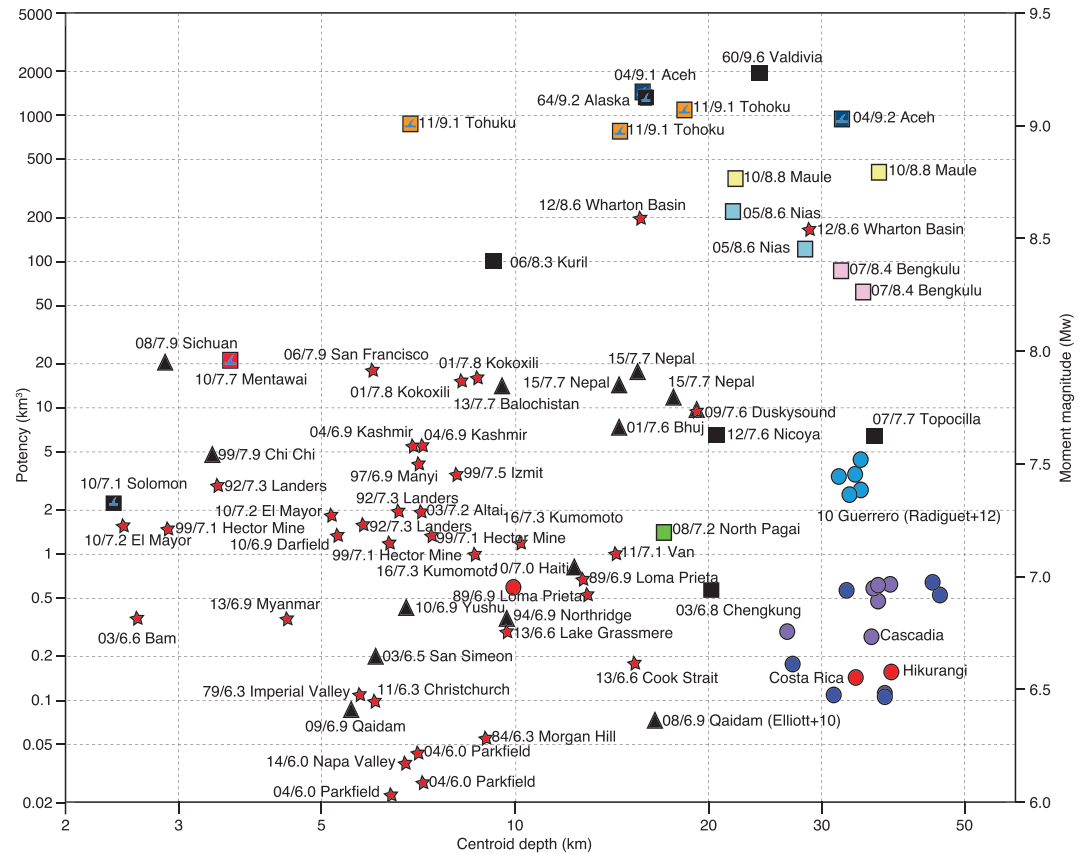


**Figure 6.** Variation of potency with centroid depth for all events in the catalog. Moment magnitude is computed using a uniform rigidity of 30 GPa. There is no apparent relationship between potency and centroid depth, considering events within similar tectonic settings or rupture styles.

The deep slow-slip events, which represent the widest ruptures of the catalog despite their small magnitude, scatter along the same trend as other type of events across various tectonic contexts. Since the source mechanism of slow and fast earthquakes may be widely different, this result indicates that similar scaling of source properties can be obtained for different events, but for different reasons. For example, Cattania and Segall (2018) discuss how the relationships among magnitude, duration, and stress drop can be similar in numerical simulations of seismic cycles, but for different underlying reasons. Slow-slip events have been found to follow the same moment-duration scaling as fast ruptures (Michel et al., 2019), despite their widely different radiation efficiency.

The large variations of potency density across tectonic settings and depth can be due to the activation of different rupture processes. For instance, the high potency density observed for continental subduction zone earthquakes and tsunami earthquakes may be attributed to strong weakening mechanisms such as flash weakening (Beeler et al., 2008; Goldsby & Tullis, 2011; Hirose & Bystricky, 2007; Kitajima et al., 2011) and thermal pressurization (Andrews, 2002; Hirose & Bystricky, 2007; Mitsui et al., 2012; Noda & Lapusta, 2013; Viesca & Garagash, 2015). The potency density of such events may be approximated with

$$\epsilon \propto \frac{\Delta\mu\bar{\sigma}}{2G}, \quad (9)$$

where  $0.1 \lesssim \Delta\mu \lesssim 0.6$  represents a large drop of frictional strength (e.g., Toro et al., 2004, 2006) and  $60 \lesssim \bar{\sigma} \lesssim 100$  MPa is the effective normal stress, leading to potency density of the order of 100 to 500 microstrain. Hence, ruptures with potency density larger than about 100 microstrain may be associated with strong weakening. This would imply that most continental strike-slip fault and continental thrust ruptures operate under this condition, compatible with the claims of Viesca and Garagash (2015). Smaller potency densities

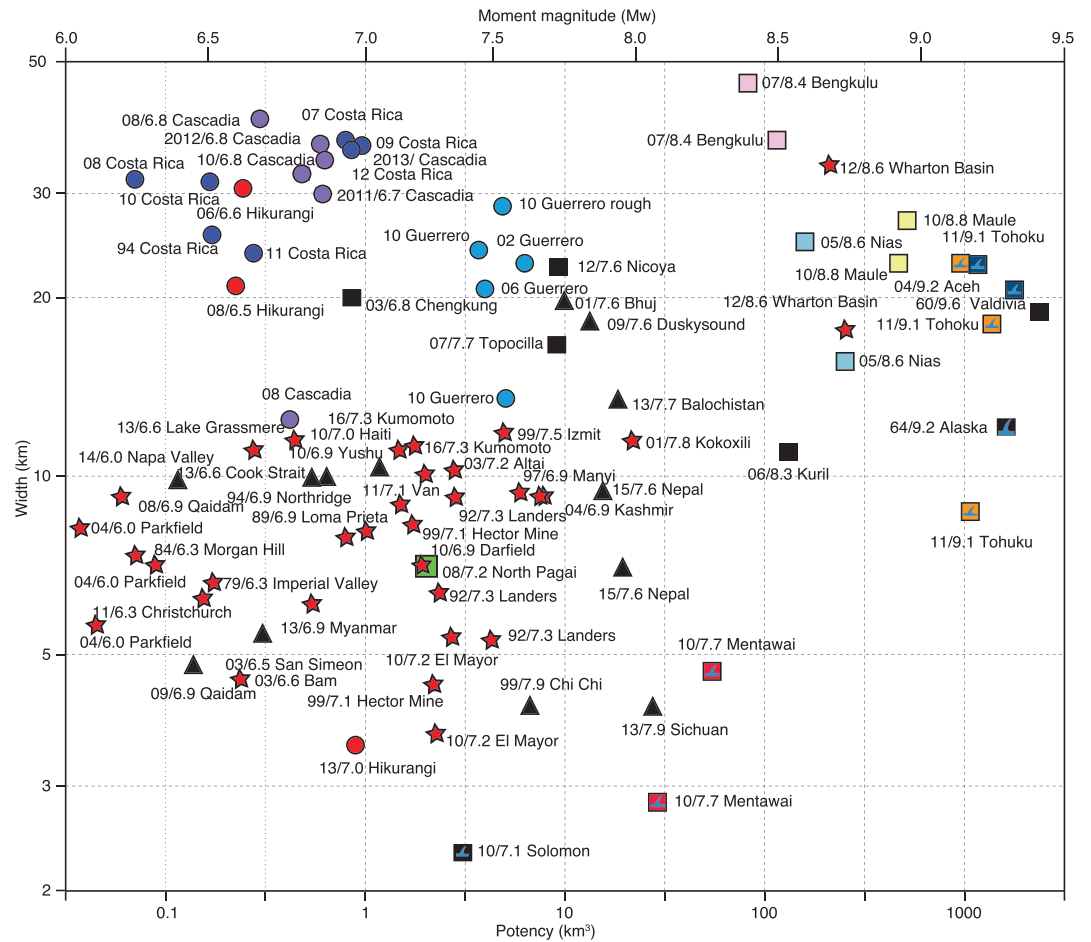


**Figure 7.** Variation of potency with width in the depth direction for all events in the catalog. Rupture size, that is, potency or moment magnitude, does not seem to control rupture width, even considering events of similar tectonic setting or rupture style.

may be explained in the framework of rate-and-state friction (Barbot, 2019a; Dieterich, 1979; Ruina, 1983) following

$$\epsilon \propto \frac{(b-a)\bar{\sigma}}{2G}, \quad (10)$$

where  $(b-a) \sim 4 \times 10^{-3}$  is the steady-state parameters controlling the velocity dependence of friction (Lapusta & Barbot, 2012; Scholz, 1998), or simply  $1 \lesssim (b-a)\bar{\sigma} \lesssim 10$  MPa, leading to a potency density in the range of 15 to 150 microstrain. However, this estimate may vary greatly because of dynamic stress overshoot or undershoot (Kanamori & Rivera, 2006) and the detailed geometry of a rupture. Slow-slip events occur in the stable weakening regime, corresponding to failed nucleations (Barbot, 2019b; Bürgmann, 2018; Goswami & Barbot, 2018; Liu & Rice, 2005, 2007; Segall et al., 2010). Hence, their total slip scales with the characteristic weakening distance, as in

$$\epsilon \propto \frac{L}{R}, \quad (11)$$

where  $1 \lesssim L \lesssim 10$  cm is the characteristic weakening distance of rate-and-state friction in a range compatible with slow slip and  $R \sim 50$  km is the down-dip rupture width, leading to estimates of potency density in the range of 0.01 to 3 microstrain. The overall variability of source properties, for example, two orders of magnitude for potency density, may be attributed to the presence of frictional contrast along the fault (Kaneko et al., 2010; Kaneko & Shearer, 2015), variability of earthquake slip due to the stress shadow of previous ruptures (Barbot, 2019b; Michel et al., 2017; Van Dither et al., 2013), morphological gradients (Qiu et al., 2016; Sathiakumar et al., 2020), variation of off-fault damage (Cappa et al., 2014), differing coupling coefficients

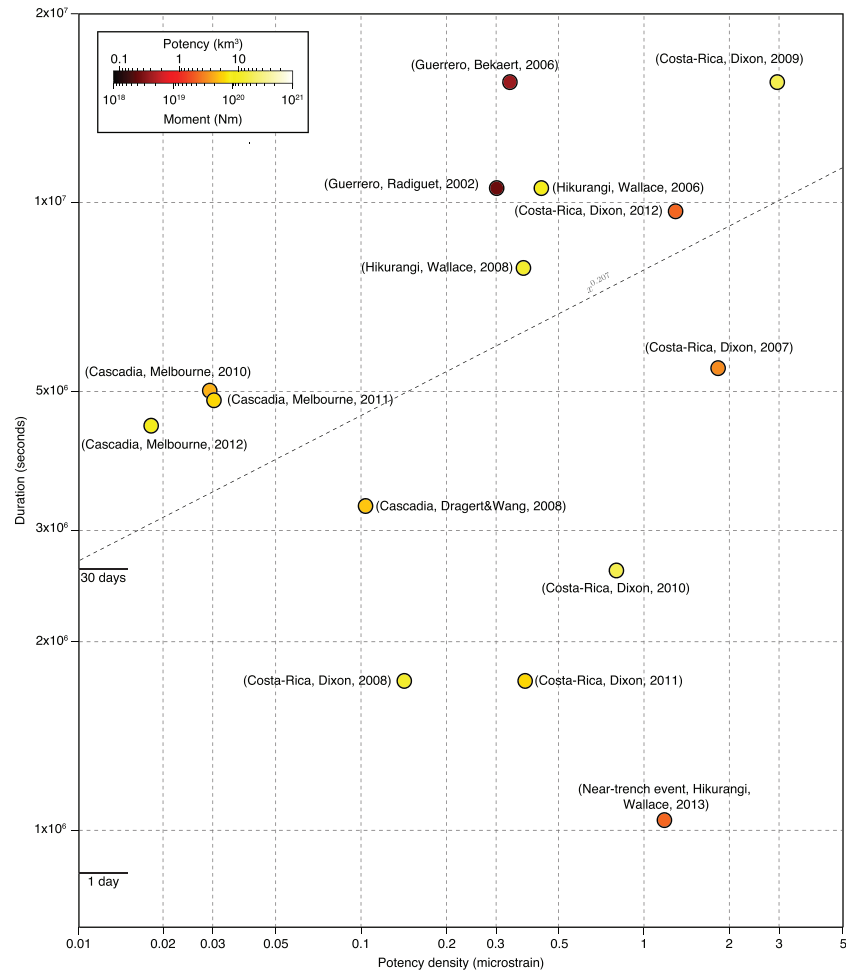


**Figure 8.** Variation of potency density with event duration for all the slow-slip events in the catalog. The duration of events scales sublinearly with potency density as  $x^{-0.276}$ . The 2013 Hikurangi event is an outlier, presumably due to its shallow centroid depth, pointing to a different rupture mechanism than for deeper events.

(Chounet & Vallée, 2018), or the activation of different weakening mechanisms (Cocco et al., 2016; Cattania & Segall, 2018; Kirkpatrick & Shipton, 2009).

The variability of potency density among events has important implications on the moment-duration scaling relationship of slow-slip events, which may differ from that of fast ruptures (Peng & Gombert, 2010). Simple models provide a rationale to understand the moment-duration scaling of slow and fast ruptures. For slow-slip events, we may assume that the rupture spreads rapidly across a fixed down-dip width  $W$  and then propagates along strike for most of the duration of the event at a constant rupture velocity between 0.01 and 0.1 m/s. This leads to the along-strike rupture length  $L = V_r T$  and the rupture area  $A = W V_r T$ , where  $V_r$  is the rupture velocity and  $T$  is the rupture duration. The relationship between slip and potency density  $s \approx \epsilon W$  also holds. The moment released by slow-slip events can then be defined as

$$M \approx GWV_r \epsilon T, \quad (12)$$

showing a linear relationship among moment, duration, and potency density. For fast ruptures, a simple model assumes a linear relationship between rupture duration and rupture radius, leading to

$$M \approx GV_r^3 \epsilon T^3, \quad (13)$$

which shows a power law between moment and duration. More sophisticated models of fast ruptures that incorporate the propagation of aseismic slip into the rupture area provide slightly different power exponents (Cattania & Segall, 2018; Chen & Lapusta, 2009). Deciphering the moment-duration scaling for slow-slip

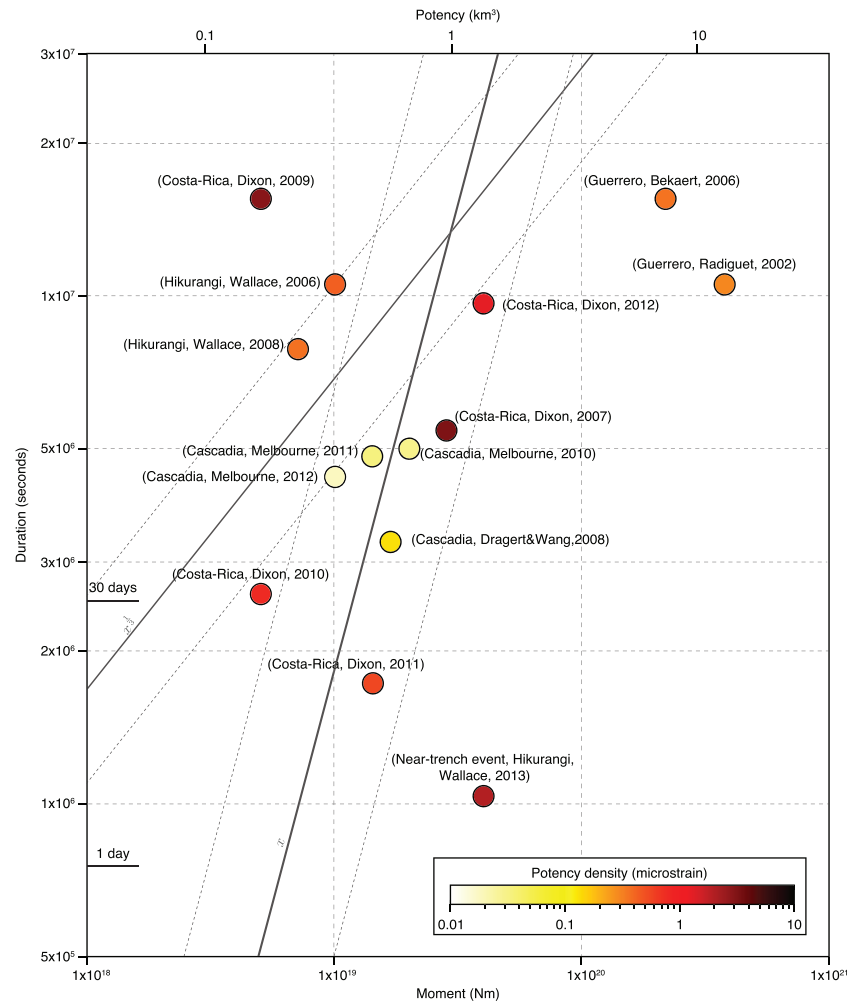


**Figure 9.** Variation of moment with event duration for all the slow-slip events in the catalog. All the events appear to neither favor the  $M \propto T$  nor the  $M \propto T^3$  scaling law, whether considering individual regions or all the events together.

events is important to better understand the underlying source processes. However, large variations of potency density of about two orders of magnitude (Figures 3 and 4) can introduce important bias if potency density is not included in the analysis. This may explain the contradictory results found at the Cascadia subduction zone, where Gao et al. (2012) and Michel et al. (2019) found linear and cubic moment-duration scalings, respectively, for events rupturing similar sections of the Cascadia megathrust. To shed more light on this problem, we investigate the relationship among moment, duration, and potency density with the catalog of slow-slip events. For the collection of slow-slip events considered, the duration ranges between 7 days and 180 days, the moment covers 2 orders of magnitude, between  $5 \times 10^{18}$  to  $5 \times 10^{20}$  Nm, and the potency density varies between 0.01 and 3 microstrains, providing a sufficient dynamic range to investigate the scaling relationships. Event duration increases with potency density, with  $T \approx \epsilon^{0.2}$  for the entire catalog (Figure 8). The largest outlier corresponds to a near-trench event at the Hikurangi subduction zone that may involve a different rupture mechanism than its deep counterparts. The moment-duration relationship (Figure 9) shows large variability that cannot be reduced by either the linear and cubic root scaling laws, whether or not regions are considered individually or together. We conclude that variations in potency density among slow-slip events preclude a simple characterization in terms of a linear or cubic root scaling between moment and duration. Several micro-physical mechanisms of deformation may be responsible for the slow-slip phenomenon, including stable weakening (Liu & Rice, 2005, 2007; Veedu & Barbot, 2016), dilatant hardening (Segall et al., 2010), semi-brittle deformation (Goswami & Barbot, 2018), fluid pulses (Cruz-Atienza et al., 2018), and thermal instabilities (Wang & Barbot, 2020). In addition, some slow-slip events do not occur spontaneously but are triggered by distant seismic events (Zigone et al., 2012). It is

possible that a single scaling relationship may be inadequate to capture a such wide range of rupture mechanisms. In addition, a constant rupture velocity may not be applicable during nucleation, propagation, and arrest of slow-slip ruptures (Dal Zilio et al., 2020).

## 5. Conclusion

We gather a catalog of slow and fast earthquake slip distributions derived from the analysis of geodetic and other geophysical data to better understand the static source properties of continental and subduction earthquakes and slow-slip events. We estimate simple source characteristics, such as centroid depth, width, potency, and potency density, with limited bias from unknown variability of elastic properties. This allows us to compare events of different styles from various tectonic settings and source depths. The potency density, a fundamental property of ruptures related to stress drop affecting rupture size and rupture style, varies significantly depending on the tectonic setting and, in the case of megathrust earthquakes, centroid depth. In particular, the potency density of shallow earthquakes and tsunami earthquakes is higher than their deep counterpart. This implies systematic variation of rupture processes with depth on a megathrust, with strong weakening being more prominent closer to the trench. Deep megathrust earthquake share a lower potency density, indicative of less efficient weakening mechanisms or the propagation of deep ruptures into stable-weakening regions. Slow-slip events at subduction zones represent an end-member of large ruptures characterized with low potency density. Large variability in potency density among slow-slip events, which affects duration, makes simple scaling relationships for the moment-duration scaling inadequate. If large potency density is indicative of strong weakening mechanisms, most continental strike-slip fault and continental thrust ruptures operate under this condition.

## Acknowledgments

The study benefited from funding from the National Science Foundation, under award number EAR-1848192. This work comprises Earth Observatory of Singapore contribution no. 336. This research was also supported by the National Research Foundation (NRF) Singapore under its NRF Fellowship scheme (award no. NRF-NRFF2013-06) and by the Earth Observatory of Singapore (EOS) and the Singapore Ministry of Education under the Research Centres of Excellence initiative.

## References

- Agata, R., Barbot, S. D., Fujita, K., Hyodo, M., Iinuma, T., Nakata, R., & Hori, T. (2019). Rapid mantle flow with power-law creep explains deformation after the 2011 Tohoku mega-quake. *Nature Communications*, *10*(1), 1385.
- Aki, K. (1967). Scaling law of seismic spectrum. *Journal of Geophysical Research*, *72*(4), 1217–1231. <https://doi.org/10.1029/JZ072i004p01217>
- Aki, K. (1979). Characterization of barriers on an earthquake fault. *Journal of Geophysical Research*, *84*(B11), 6140–6148. <https://doi.org/10.1029/JB084iB11p06140>
- Allmann, B. P., & Shearer, P. M. (2009). Global variations of stress drop for moderate to large earthquakes. *Journal of Geophysical Research*, *114*, B01310. <https://doi.org/10.1029/2008JB005821>
- Amey, R., Hooper, A., & Walters, R. (2018). A Bayesian method for incorporating self-similarity into earthquake slip inversions. *Journal of Geophysical Research: Solid Earth*, *123*, 6052–6071. <https://doi.org/10.1029/2017JB015316>
- Andrews, D. (2002). A fault constitutive relation accounting for thermal pressurization of pore fluid. *Journal of Geophysical Research*, *107*(B12), ESE–15. <https://doi.org/10.1029/2002JB001942>
- Aster, R. C., Borchers, B., & Thurber, C. H. (2012). Parameter estimation and inverse problems.
- Atzori, S., & Antonioli, A. (2011). Optimal fault resolution in geodetic inversion of coseismic data. *Geophysical Journal International*, *185*(1), 529–538. <https://doi.org/10.1111/j.1365-246X.2011.04955.x>
- Avouac, J. P., Ayoub, F., Leprince, S., Konca, O., & Helmberger, D. V. (2006). The 2005, Mw 7.6 Kashmir earthquake: Sub-pixel correlation of ASTER images and seismic waveforms analysis. *Earth and Planetary Science Letters*, *249*(3–4), 514–528. <https://doi.org/10.1016/j.epsl.2006.06.025>
- Avouac, J. P., Ayoub, F., Wei, S., Ampuero, J. P., Meng, L., Leprince, S., & Helmberger, D. (2014). The 2013, Mw 7.7 Balochistan earthquake, energetic strike-slip reactivation of a thrust fault. *Earth and Planetary Science Letters*, *391*, 128–134. <https://doi.org/10.1016/j.epsl.2014.01.036>
- Avouac, J. P., Meng, L., Wei, S., Wang, T., & Ampuero, J. P. (2015). Lower edge of locked Main Himalayan Thrust unzipped by the 2015 Gorkha earthquake. *Nature Geoscience*, *8*, 708–711. <https://doi.org/10.1038/ngeo2518>
- Baltay, A., & Hanks, T. C. (2014). Understanding the magnitude dependence of PGA and PGV in NGA-West 2 data. *Bulletin of the Seismological Society of America*, *104*(6), 2851–2865. <https://doi.org/10.1785/0120130283>
- Baltay, A., Ide, S., Prieto, G., & Beroza, G. (2011). Variability in earthquake stress drop and apparent stress. *Geophysical Research Letters*, *38*, L06303. <https://doi.org/10.1029/2011GL046698>
- Barbot, S. (2019a). Modulation of fault strength during the seismic cycle by grain-size evolution around contact junctions. *Tectonophysics*, *765*, 129–145. <https://doi.org/10.1016/j.tecto.2019.05.004>
- Barbot, S. (2019b). Slow-slip, slow earthquakes, period-two cycles, full and partial ruptures, and deterministic chaos in a single asperity fault. *Tectonophysics*, *768*, 228, 171. <https://doi.org/10.1016/j.tecto.2019.228171>
- Barbot, S. (2020). Frictional and structural controls of seismic super-cycles at the Japan trench. *Earth Planets Space*, *72*, 63.
- Barbot, S., Agram, P., & De Michele, M. (2013). Change of apparent segmentation of the San Andreas fault around Parkfield from space geodetic observations across multiple periods. *Journal of Geophysical Research: Solid Earth*, *118*, 6311–6327. <https://doi.org/10.1002/2013JB010442>
- Barbot, S., & Fialko, Y. (2010). A unified continuum representation of postseismic relaxation mechanisms: Semi-analytic models of afterslip, poroelastic rebound and viscoelastic flow. *Geophysical Journal International*, *182*(3), 1124–1140. <https://doi.org/10.1111/j.1365-246X.2010.04678.x>
- Barbot, S., Fialko, Y., & Bock, Y. (2009). Postseismic deformation due to the Mw 6.0 2004 Parkfield earthquake: Stress-driven creep on a fault with spatially variable rate-and-state friction parameters. *Journal of Geophysical Research*, *114*, B07405. <https://doi.org/10.1029/2008JB005748>

- Barbot, S., Hamiel, Y., & Fialko, Y. (2008). Space geodetic investigation of the coseismic and postseismic deformation due to the 2003 Mw 7.2 Altai earthquake: Implications for the local lithospheric rheology. *Journal of Geophysical Research*, *113*, B03403. <https://doi.org/10.1029/2007JB005063>
- Barbot, S., Lapusta, N., & Avouac, J. P. (2012). Under the hood of the earthquake machine: Toward predictive modeling of the seismic cycle. *Science*, *336*(6082), 707–710. <https://doi.org/10.1126/science.1218796>
- Bechor, N. B. D., & Zebker, H. A. (2006). Measuring two-dimensional movements using a single InSAR pair. *Geophysical Research Letters*, *33*, L16311. <https://doi.org/10.1029/2006GL026883>
- Beeler, N., Hickman, S., & Wong, T. F. (2001). Earthquake stress drop and laboratory-inferred interseismic strength recovery. *Journal of Geophysical Research*, *106*(B12), 30,701–30,713. <https://doi.org/10.1029/2000JB900242>
- Beeler, N. M., Tullis, T. E., & Goldsby, D. L. (2008). Constitutive relationship and physical basis of fault strength due to flash heating. *Journal of Geophysical Research*, *113*, B01401. <https://doi.org/10.1029/2007JB004988>
- Bejar Pizarro, M., Carrizo, D., Socquet, A., & Armijo, R. (2010). Asperities, barriers and transition zone in the North Chile seismic gap: State of the art after the 2007 Mw 7.7 Tocopilla earthquake inferred by GPS and InSAR data. ESA Special Publication (Vol. 677).
- Bekaert, D., Hooper, A., & Wright, T. (2015). Reassessing the 2006 Guerrero slow-slip event, Mexico: Implications for large earthquakes in the Guerrero gap. *Journal of Geophysical Research: Solid Earth*, *120*, 1357–1375. <https://doi.org/10.1002/2014JB011557>
- Ben-Zion, Y. (2001). On quantification of the earthquake source. *Seismological Research Letters*, *72*(2), 151–152. <https://doi.org/10.1785/gssrl.72.2.151>
- Ben-Zion, Y., Lee, W., Kanamori, H., Jennings, P., & Kisslinger, C. (2003). Key formulas in earthquake seismology. *International Handbook of Earthquake and Engineering Seismology*, *81*, 1857–1875.
- Ben-Zion, Y., & Lyakhovskiy, V. (2019). Representation of seismic sources sustaining changes of elastic moduli. *Geophysical Journal International*, *217*(1), 135–139. <https://doi.org/10.1093/gji/ggz018>
- Ben-Zion, Y., & Zhu, L. (2002). Potency-magnitude scaling relations for southern California earthquakes with  $1.0 < M_L < 7.0$ . *Geophysical Journal International*, *148*(3), F1–F5. <https://doi.org/10.1046/j.1365-246X.2002.01637.x>
- Beroza, G. C., & Ide, S. (2011). Slow earthquakes and nonvolcanic tremor. *Annual Review of Earth and Planetary Sciences*, *39*(1), 271–296. <https://doi.org/10.1146/annurev-earth-040809-152531>
- Beroza, G. C., & Spudich, P. (1988). Linearized inversion for fault rupture behavior: Application to the 1984 Morgan Hill, California, earthquake. *Journal of Geophysical Research*, *93*(B6), 6275. <https://doi.org/10.1029/JB093iB06p06275>
- Bilek, S. L., Engdahl, E. R., DeShon, H. R., & El Hariri, M. (2011). The 25 October 2010 Sumatra tsunami earthquake: Slip in a slow patch. *Geophysical Research Letters*, *38*, L14306. <https://doi.org/10.1029/2011GL047864>
- Bilek, S. L., & Lay, T. (2002). Tsunami earthquakes possibly widespread manifestations of frictional conditional stability. *Geophysical Research Letters*, *29*(14), 1673. <https://doi.org/10.1029/2002GL015215>
- Bletery, Q., Sladen, A., Delouis, B., Vallée, M., Nocquet, J. M., Rolland, L., & Jiang, J. (2014). A detailed source model for the Mw 9.0 Tohoku-Oki earthquake reconciling geodesy, seismology and tsunami records. *Journal of Geophysical Research: Solid Earth*, *119*, 7636–7653. <https://doi.org/10.1002/2014JB011261>
- Brengman, C. M., Barnhart, W. D., Mankin, E. H., & Miller, C. N. (2019). Earthquake-scaling relationships from geodetically derived slip distributions. *Bulletin of the Seismological Society of America*, *109*(5), 1701–1715. <https://doi.org/10.1785/0120190048>
- Brown, L., Wang, K., & Sun, T. (2015). Static stress drop in the Mw 9 Tohoku-oki earthquake: Heterogeneous distribution and low average value. *Geophysical Research Letters*, *42*, 10,595–10,600. <https://doi.org/10.1002/2015GL066361>
- Brune, J. (1970). Tectonic stress and the spectra of seismic shear waves from earthquakes. *Journal of Geophysical Research*, *75*, 4997–5009. <https://doi.org/10.1029/JB075i026p04997>
- Bürgmann, R. (2018). The geophysics, geology and mechanics of slow fault slip. *Earth and Planetary Science Letters*, *495*, 112–134. <https://doi.org/10.1016/j.epsl.2018.04.062>
- Cappa, F., Perrin, C., Manighetti, I., & Delor, E. (2014). Off-fault long-term damage: A condition to account for generic, triangular earthquake slip profiles. *Geochemistry, Geophysics, Geosystems*, *15*, 1476–1493. <https://doi.org/10.1002/2013GC005182>
- Cattania, C., & Segall, P. (2018). Crack models of repeating earthquakes predict observed moment-recurrence scaling. *Journal of Geophysical Research*, *124*, 476–503. <https://doi.org/10.1029/2018JB016056>
- Chen, T., & Lapusta, N. (2009). Scaling of small repeating earthquakes explained by interaction of seismic and aseismic slip in a rate and state fault model. *Journal of Geophysical Research*, *114*, B01311. <https://doi.org/10.1029/2008JB005749>
- Chlieh, M., Avouac, J. P., Hjorleifsdottir, V., Song, T. R. A., Ji, C., Sieh, K., & Galetzka, J. (2007). Coseismic slip and afterslip of the great Mw 9.15 Sumatra-Andaman earthquake of 2004. *Bulletin of the Seismological Society of America*, *97*(1A), S152–S173. <https://doi.org/10.1785/0120050631>
- Chounet, A., & Vallée, M. (2018). Global and interregion characterization of subduction interface earthquakes derived from source time functions properties. *Journal of Geophysical Research: Solid Earth*, *123*, 5831–5852. <https://doi.org/10.1029/2018JB015932>
- Cocco, M., Tinti, E., & Cirella, A. (2016). On the scale dependence of earthquake stress drop. *Journal of Seismology*, *20*(4), 1151–1170. <https://doi.org/10.1007/s10950-016-9594-4>
- Copley, A., Avouac, J. P., Hollingsworth, J., & Leprince, S. (2011). The 2001 Mw 7.6 Bhuj earthquake, low fault friction, and the crustal support of plate driving forces in India. *Journal of Geophysical Research*, *116*, B08405. <https://doi.org/10.1029/2010JB008137>
- Courboux, F., Vallée, M., Causse, M., & Chounet, A. (2016). Stress-drop variability of shallow earthquakes extracted from a global database of source time functions. *Seismological Research Letters*, *87*(4), 912–918. <https://doi.org/10.1785/0220150283>
- Cruz-Atienza, V. M., Villafuerte, C., & Bhat, H. S. (2018). Rapid tremor migration and pore-pressure waves in subduction zones. *Nature Communications*, *9*(1), 2900. <https://doi.org/10.1038/s41467-018-05150-3>
- Dal Zilio, L., Lapusta, N., & Avouac, J. P. (2020). Unraveling scaling properties of slow-slip events. *Geophysical Research Letters*, *47*, e2020GL087477. <https://doi.org/10.1029/2020GL087477>
- DeVries, P. M., Krastev, P. G., Dolan, J. F., & Meade, B. J. (2017). Viscoelastic block models of the North Anatolian Fault: A unified earthquake cycle representation of pre- and postseismic geodetic observations. *Bulletin of the Seismological Society of America*, *107*(1), 403–417. <https://doi.org/10.1785/0120160059>
- Dieterich, J. H. (1979). Modeling of rock friction 1. Experimental results and constitutive equations. *Journal of Geophysical Research*, *84*(B5), 2161–2168. <https://doi.org/10.1029/JB084iB05p02161>
- Dixon, T. H., Jiang, Y., Malservisi, R., McCaffrey, R., Voss, N., Protti, M., & Gonzalez, V. (2014). Earthquake and tsunami forecasts: Relation of slow slip events to subsequent earthquake rupture. *Proceedings of the National Academy of Sciences*, *111*(48), 17,039–17,044. <https://doi.org/10.1073/pnas.1412299111>
- Dragert, H., & Wang, K. (2011). Temporal evolution of an episodic tremor and slip event along the northern Cascadia margin. *Journal of Geophysical Research*, *116*, B12406. <https://doi.org/10.1029/2011JB008609>

- Dreger, D. S., Gee, L., Lombard, P., Murray, M. H., & Romanowicz, B. (2005). Rapid finite-source analysis and near-fault strong ground motions: Application to the 2003 Mw 6.5 San Simeon and 2004 Mw 6.0 Parkfield earthquakes. *Seismological Research Letters*, 76(1), 40–48. <https://doi.org/10.1785/gssrl.76.1.40>
- Duputel, Z., Agram, P. S., Simons, M., Minson, S. E., & Beck, J. L. (2014). Accounting for prediction uncertainty when inferring subsurface fault slip. *Geophysical Journal International*, 197(1), 464–482.
- Elliott, J. R., Copley, A. C., Holley, R., Scharer, K., & Parsons, B. (2013). The 2011 Mw 7.1 Van (Eastern Turkey) earthquake. *Journal of Geophysical Research: Solid Earth*, 118, 1619–1637. <https://doi.org/10.1002/jgrb.50117>
- Elliott, J. R., Nissen, E. K., England, P. C., Jackson, J. A., Lamb, S., Li, Z., & Parsons, B. (2012). Slip in the 2010–2011 Canterbury earthquakes, New Zealand. *Journal of Geophysical Research*, 117, B03401. <https://doi.org/10.1029/2011JB008868>
- Elliott, J. R., Parsons, B., Jackson, J. A., Shan, X., Sloan, R. A., & Walker, R. T. (2011). Depth segmentation of the seismogenic continental crust: The 2008 and 2009 Qaidam earthquakes. *Geophysical Research Letters*, 38, L06305. <https://doi.org/10.1029/2011GL046897>
- Eshelby, J. D. (1957). The determination of the elastic field of an ellipsoidal inclusion, and related problems. *Proceedings of the Royal Society of London. Series A. Mathematical and Physical Sciences*, 241(1226), 376–396. <https://doi.org/10.1098/rspa.1957.0133>
- Evans, E. L., & Meade, B. J. (2012). Geodetic imaging of coseismic slip and postseismic afterslip: Sparsity promoting methods applied to the great Tohoku earthquake. *Geophysical Research Letters*, 39, L11314. <https://doi.org/10.1029/2012GL051990>
- Feng, L., Hill, E. M., Elósegui, P., Qiu, Q., Hermawan, I., Banerjee, P., & Sieh, K. (2015). Hunt for slow slip events along the Sumatran subduction zone in a decade of continuous GPS data. *Journal of Geophysical Research: Solid Earth*, 120, 8623–8632. <https://doi.org/10.1002/2015JB012503>
- Feng, W., Samsonov, S., Almeida, R., Yassaghi, A., Li, J., Qiu, Q., & Zheng, W. (2018). Geodetic constraints of the 2017 Mw 7.3 Sarpol Zahab, Iran earthquake, and its implications on the structure and mechanics of the northwest Zagros thrust-fold belt. *Geophysical Research Letters*, 45, 6853–6861. <https://doi.org/10.1029/2018GL078577>
- Fialko, Y. (2004). Probing the mechanical properties of seismically active crust with space geodesy: Study of the co-seismic deformation due to the 1992  $M_w$  7.3 Landers (Southern California) earthquake. *Journal of Geophysical Research*, 109, B03307. <https://doi.org/10.1029/2003JB002756>
- Fialko, Y., Sandwell, D., Simons, M., & Rosen, P. (2005). Three-dimensional deformation caused by the Bam, Iran, earthquake and the origin of shallow slip deficit. *Nature*, 435, 295–299. <https://doi.org/10.1038/nature03425>
- Fialko, Y., Simons, M., & Agnew, D. (2001). The complete (3-D) surface displacement field in the epicentral area of the 1999  $M_w$  7.1 Hector Mine earthquake, southern California, from space geodetic observations. *Geophysical Research Letters*, 28, 3063–3066. <https://doi.org/10.1029/2001GL013174>
- Fujiwara, T., Kodaira, S., No, T., Kaiho, Y., Takahashi, N., & Kaneda, Y. (2011). The 2011 Tohoku-Oki earthquake: Displacement reaching the trench axis. *Science*, 334(6060), 1240–1240. <https://doi.org/10.1126/science.1211554>
- Fukahata, Y., & Wright, T. J. (2008). A non-linear geodetic data inversion using ABIC for slip distribution on a fault with an unknown dip angle. *Geophysical Journal International*, 173(2), 353–364. <https://doi.org/10.1111/j.1365-246X.2007.03713.x>
- Funning, G. J., Fukahata, Y., Yagi, Y., & Parsons, B. (2014). A method for the joint inversion of geodetic and seismic waveform data using ABIC: Application to the 1997 Manyi, Tibet, earthquake. *Geophysical Journal International*, 196(3), 1564–1579. <https://doi.org/10.1093/gji/ggt406>
- Gao, H., Schmidt, D. A., Ji, R. J. W., & Weldon, R. J. (2012). Scaling relationships of source parameters for slow slip events. *Bulletin of the Seismological Society of America*, 102(1), 352–360. <https://doi.org/10.1785/0120110096>
- Geersen, J. (2019). Sediment-starved trenches and rough subducting plates are conducive to tsunami earthquakes. *Tectonophysics*, 762, 28–44. <https://doi.org/10.1016/j.tecto.2019.04.024>
- Goldsby, D., & Tullis, T. E. (2011). Flash heating leads to low frictional strength of crustal rocks at earthquake slip rates. *Science*, 334(6053), 216–218. <https://doi.org/10.1126/science.1207902>
- Gomberg, J., Wech, A., Creager, K., Obara, K., & Agnew, D. (2016). Reconsidering earthquake scaling. *Geophysical Research Letters*, 43, 6243–6251. <https://doi.org/10.1002/2016GL069967>
- Gombert, B., Duputel, Z., Jolivet, R., Doubre, C., Rivera, L., & Simons, M. (2017). Revisiting the 1992 Landers earthquake: A Bayesian exploration of co-seismic slip and off-fault damage. *Geophysical Journal International*, 212(2), 839–852. <https://doi.org/10.1093/gji/ggx455>
- Gombert, B., Duputel, Z., Jolivet, R., Simons, M., Jiang, J., Liang, C., & Rivera, L. (2018). Strain budget of the Ecuador-Colombia subduction zone: A stochastic view. *Earth and Planetary Science Letters*, 498, 288–299.
- Goodner, H. L. (2014). Spatial Relationship Between GPS Slip and Seismic Tremor During Cascadia Slow Slip Events (Doctoral dissertation). Central Washington University.
- Goswami, A., & Barbot, S. (2018). Slow-slip events in semi-brittle serpentinite fault zones. *Scientific Reports*, 8(1), 6181. <https://doi.org/10.1038/s41598-018-24637-z>
- Gusman, A. R., Murotani, S., Satake, K., Heidarzadeh, M., Gunawan, E., Watada, S., & Schurr, B. (2015). Fault slip distribution of the 2014 Iquique, Chile, earthquake estimated from ocean-wide tsunami waveforms and GPS data. *Geophysical Research Letters*, 42, 1053–1060. <https://doi.org/10.1002/2014GL062604>
- Hamling, I. J., D’Anastasio, E., Wallace, L. M., Ellis, S., Motagh, M., Samsonov, S., & Hreinsdóttir, S. (2014). Crustal deformation and stress transfer during a propagating earthquake sequence: The 2013 Cook Strait sequence, central New Zealand. *Journal of Geophysical Research: Solid Earth*, 119, 6080–6092. <https://doi.org/10.1002/2014JB011084>
- Hang, Y., Barbot, S., Dauwels, J., T., W., Nanjundiah, P., & Qiu, Q. (2020). Outlier-insensitive Bayesian inference for linear inverse problems (OutBI) with applications to space geodetic data. *Geophysical Journal International*, 221, 334–350. <https://doi.org/10.1093/gji/ggz559>
- Hernandez, B., Cotton, F., & Campillo, M. (1999). Contribution of radar interferometry to a two-step inversion of the kinematic process of the 1992 Landers earthquake. *Journal of Geophysical Research*, 104(B6), 13,083–13,099. <https://doi.org/10.1029/1999JB900078>
- Herrendörfer, R., van Dinther, Y., Gerya, T., & Dalguer, L. A. (2015). Earthquake supercycle in subduction zones controlled by the width of the seismogenic zone. *Nature Geoscience*, 8(6), 471–474. <https://doi.org/10.1038/ngeo2427>
- Hill, E. M., Yue, H., Barbot, S., Lay, T., Tapponnier, P., Hermawan, I., & Sieh, K. (2015). The 2012  $M_w$  8.6 Wharton Basin sequence: A cascade of great earthquakes generated by near-orthogonal, young, oceanic mantle faults. *Journal of Geophysical Research: Solid Earth*, 120, 3723–3747. <https://doi.org/10.1002/2014JB011703>
- Hirose, T., & Bystricky, M. (2007). Extreme dynamic weakening of faults during dehydration by coseismic shear heating. *Geophysical Research Letters*, 34, L14311. <https://doi.org/10.1029/2007GL030049>
- Hirth, G., & Kohlstedt, D. L. (1995). Experimental constraints on the dynamics of the partially molten upper mantle: 2. Deformation in the dislocation creep regime. *Journal of Geophysical Research*, 100(B8), 15,441–15,449.

- Hoechner, A., Sobolev, S. V., Einarsson, I., & Wang, R. (2011). Investigation on afterslip and steady state and transient rheology based on postseismic deformation and geoid change caused by the Sumatra 2004 earthquake. *Geochemistry, Geophysics, Geosystems*, *12*, Q07010. <https://doi.org/10.1029/2010GC003450>
- Hudnut, K., Shen, Z., Murray, M., McClusky, S., King, R., & Herring, T. (1996). Co-seismic displacements of the 1994 Northridge, California, earthquake. *Bulletin of the Seismological Society of America*, *86*(1B), S19–S36.
- Iinuma, T., Hino, R., Kido, M., Inazu, D., Osada, Y., & Ito, Y. (2012). Coseismic slip distribution of the 2011 off the Pacific Coast of Tohoku Earthquake (M9.0) refined by means of seafloor geodetic data. *Journal of Geophysical Research*, *117*, B07409. <https://doi.org/10.1029/2012JB009186>
- Ishii, M., Shearer, P. M., Houston, H., & Vidale, J. E. (2005). Extent, duration and speed of the 2004 Sumatra-Andaman earthquake imaged by the Hi-Net array. *Nature*, *435*(7044), 933. <https://doi.org/10.1038/nature03675>
- Ji, C., Larson, K. M., Tan, Y., Hudnut, K. W., & Choi, K. (2004). Slip history of the 2003 San Simeon earthquake constrained by combining 1-Hz GPS, strong motion, and teleseismic data. *Geophysical Research Letters*, *31*, L17608. <https://doi.org/10.1029/2004GL020448>
- Jiang, J., & Simons, M. (2016). Probabilistic imaging of tsunamigenic seafloor deformation during the 2011 Tohoku-oki Earthquake. *Journal of Geophysical Research: Solid Earth*, *121*, 9050–9076. <https://doi.org/10.1002/2016JB013760>
- Jiang, Y., Wdowinski, S., Dixon, T. H., Hackl, M., Protti, M., & Gonzalez, V. (2012). Slow slip events in Costa Rica detected by continuous GPS observations, 2002–2011. *Geochemistry, Geophysics, Geosystems*, *13*, Q04006. <https://doi.org/10.1029/2012GC004058>
- Johnson, J. M., Satake, K., Holdahl, S. R., & Sauber, J. (1996). The 1964 Prince William Sound earthquake: Joint inversion of tsunami and geodetic data. *Journal of Geophysical Research*, *101*(B1), 523–532. <https://doi.org/10.1029/95jb02806>
- Kanamori, H. (1972). Mechanism of tsunami earthquake. *Physics of the Earth and Planetary Interiors*, *6*, 346–359. [https://doi.org/10.1016/0031-9201\(72\)90058-1](https://doi.org/10.1016/0031-9201(72)90058-1)
- Kanamori, H., & Anderson, D. (1975). Theoretical basis for some empirical relations in Seismology. *Bulletin of the Seismological Society of America*, *65*(5), 213–220.
- Kanamori, H., Mori, J. I. M., Hauksson, E., Heaton, T. H., Hutton, K., & Jones, L. M. (1993). Determination of earthquake energy release and ML using terrascopes. *Bulletin of the Seismological Society of America*, *83*(2), 330–346.
- Kanamori, H., & Rivera, L. (2006). Energy partitioning during an earthquake. In R. Abercrombie, A. McGarr, A. Kanamori, & G. D. Toro (Eds.), *Earthquakes: Radiated Energy and the Physics of Faulting* (Vol. 170, pp. 3–13). Washington D.C.: AGU.
- Kaneko, Y., Avouac, J. P., & Lapusta, N. (2010). Towards inferring earthquake patterns from geodetic observations of interseismic coupling. *Nature Geoscience*, *3*, 363–369. <https://doi.org/10.1038/ngeo843>
- Kaneko, Y., & Shearer, P. (2014). Seismic source spectra and estimated stress drop derived from cohesive-zone models of circular subshear rupture. *Geophysical Journal International*, *197*(2), 1002–1015. <https://doi.org/10.1093/gji/ggu030>
- Kaneko, Y., & Shearer, P. (2015). Variability of seismic source spectra, estimated stress drop, and radiated energy, derived from cohesive-zone models of symmetrical and asymmetrical circular and elliptical ruptures. *Journal of Geophysical Research: Solid Earth*, *120*, 1053–1079. <https://doi.org/10.1002/2014JB011642>
- Kato, N. (2012). Dependence of earthquake stress drop on critical slip-weakening distance. *Journal of Geophysical Research*, *117*, B01301. <https://doi.org/10.1029/2011JB008359>
- Kirkpatrick, J., & Shipton, Z. (2009). Geologic evidence for multiple slip weakening mechanisms during seismic slip in crystalline rock. *Journal of Geophysical Research*, *114*, B12401. <https://doi.org/10.1029/2008JB006037>
- Kitajima, H., Chester, F. M., & Chester, J. S. (2011). Dynamic weakening of gouge layers in high-speed shear experiments: Assessment of temperature-dependent friction, thermal pressurization, and flash heating. *Journal of Geophysical Research*, *116*, B08309. <https://doi.org/10.1029/2010JB007879>
- Konca, A. O., Hjørleifsdóttir, V., Song, T. R. A., Avouac, J. P., Helmlberger, D. V., Ji, C., & Meltzner, A. (2007). Rupture kinematics of the 2005 Mw 8.6 Nias-Simeulue earthquake from the joint inversion of seismic and geodetic data. *Bulletin of the Seismological Society of America*, *97*(1A), S307–S322. <https://doi.org/10.1785/0120050632>
- Lapusta, N., & Barbot, S. (2012). Models of earthquakes and aseismic slip based on laboratory-derived rate and state friction laws. In A. Bizzarri, & H. S. Bhat (Eds.), *The mechanics of faulting: From laboratory to real earthquakes* (pp. 153–207). Trivandrum, Kerala, India: Research Signpost.
- Lasserre, C., Peltzer, G., Crampé, F., Klinger, Y., Van der Woerd, J., & Tapponnier, P. (2005). Coseismic deformation of the 2001  $M_w = 7.8$  Kokoxili earthquake in Tibet, measured by synthetic aperture radar interferometry. *Journal of Geophysical Research*, *110*, B12408. <https://doi.org/10.1029/2004JB003500>
- Leeman, J., Saffer, D., Scuderi, M., & Marone, C. (2016). Laboratory observations of slow earthquakes and the spectrum of tectonic fault slip modes. *Nature Communications*, *7*, 11104. <https://doi.org/10.1038/ncomms11104>
- Li, Z., Elliott, J. R., Feng, W., Jackson, J. A., Parsons, B. E., & Walters, R. J. (2011). The 2010  $M_w$  6.8 Yushu (Qinghai, China) earthquake: Constraints provided by InSAR and body wave seismology. *Journal of Geophysical Research*, *116*, B10302. <https://doi.org/10.1029/2011JB008358>
- Liu, Y., & Rice, J. R. (2005). Aseismic slip transients emerge spontaneously in three-dimensional rate and state modeling of subduction earthquake sequences. *Journal of Geophysical Research*, *110*, B08307. <https://doi.org/10.1029/2004JB003424>
- Liu, Y., & Rice, J. R. (2007). Spontaneous and triggered aseismic deformation transients in a subduction fault model. *Journal of Geophysical Research*, *112*, B09404. <https://doi.org/10.1029/2007JB004930>
- Liu-Zeng, J., Heaton, T., & DiCaprio, C. (2005). The effect of slip variability on earthquake slip-length scaling. *Geophysical Journal International*, *162*(3), 841–849. <https://doi.org/10.1111/j.1365-246X.2005.02679.x>
- Lorenzo-Martin, F., Roth, F., & Wang, R. (2006). Inversion for rheological parameters from post-seismic surface deformation associated with the 1960 Valdivia earthquake, Chile. *Geophysical Journal International*, *164*(1), 75–87. <https://doi.org/10.1111/j.1365-246X.2005.02803.x>
- Lorito, S., Romano, F., Atzori, S., Tong, X., Avallone, A., McCloskey, J., & Piatanesi, A. (2011). Limited overlap between the seismic gap and coseismic slip of the great 2010 Chile earthquake. *Nature Geoscience*, *4*(3), 173–177. <https://doi.org/10.1038/ngeo1073>
- Loveless, J. P., & Meade, B. J. (2011). Spatial correlation of interseismic coupling and coseismic rupture extent of the 2011  $M_w = 9.0$  Tohoku-oki earthquake. *Geophysical Research Letters*, *38*, L17306. <https://doi.org/10.1029/2011GL048561>
- Luttrell, K. M., Tong, X., Sandwell, D. T., Brooks, B. A., & Bevis, M. G. (2011). Estimates of stress drop and crustal tectonic stress from the 27 February 2010 Maule, Chile, earthquake: Implications for fault strength. *Journal of Geophysical Research*, *116*, B11401. <https://doi.org/10.1029/2011JB008509>
- Madariaga, R. (1976). Dynamics of an expanding circular fault. *Bulletin of the Seismological Society of America*, *66*(3), 639–666.
- Madariaga, R. (1977). Implications of stress-drop models of earthquakes for the inversion of stress drop from seismic observations, *Stress in the Earth* pp. 301–316). Birkhäuser Verlag Basel: Springer. [https://doi.org/10.1007/978-3-0348-5745-1\\_19](https://doi.org/10.1007/978-3-0348-5745-1_19)

- Mai, P. M., & Beroza, G. C. (2000). Source scaling properties from finite-fault-rupture models. *Bulletin of the Seismological Society of America*, 90(3), 604–615. <https://doi.org/10.1785/0119990126>
- Manighetti, I., Campillo, M., Bouley, S., & Cotton, F. (2007). Earthquake scaling, fault segmentation, and structural maturity. *Earth and Planetary Science Letters*, 253(3–4), 429–438. <https://doi.org/10.1016/j.epsl.2006.11.004>
- Manighetti, I., King, G., Gaudemer, Y., Scholz, C., & Doubre, C. (2001). Slip accumulation and lateral propagation of active normal faults in Afar. *Journal of Geophysical Research*, 106, 13,667–13,696. <https://doi.org/10.1029/2000JB900471>
- McGuire, J. J., & Segall, P. (2003). Imaging of aseismic fault slip transients recorded by dense geodetic networks. *Geophysical Journal International*, 155, 778–788. <https://doi.org/10.1111/j.1365-246X.2003.02022.x>
- Michel, S., Avouac, J. P., Lapusta, N., & Jiang, J. (2017). Pulse-like partial ruptures and high-frequency radiation at creeping-locked transition during megathrust earthquakes. *Geophysical Research Letters*, 44, 8345–8351. <https://doi.org/10.1002/2017GL074725>
- Michel, S., Gualandi, A., & Avouac, J. P. (2019). Similar scaling laws for earthquakes and Cascadia slow-slip events. *Nature*, 574(7779), 522–526. <https://doi.org/10.1038/s41586-019-1673-6>
- Minson, S. E., Simons, M., Beck, J. L., Ortega, F., Jiang, J., Owen, S. E., & Sladen, A. (2014). Bayesian inversion for finite fault earthquake source models—II: The 2011 great Tohoku-oki, Japan earthquake. *Geophysical Journal International*, 198(2), 922–940. <https://doi.org/10.1093/gji/ggu170>
- Mitsui, Y., Iio, Y., & Fukahata, Y. (2012). A scenario for the generation process of the 2011 Tohoku earthquake based on dynamic rupture simulation: Role of stress concentration and thermal fluid pressurization. *Earth, Planets and Space*, 64(12), 12. <https://doi.org/10.5047/eps.2012.05.016>
- Miyakoshi, K., Somei, K., Yoshida, K., Kurahashi, S., Irikura, K., & Kamae, K. (2019). Scaling relationships of source parameters of inland crustal earthquakes in tectonically active regions. *Pure and Applied Geophysics*, 117, 1917–1929. <https://doi.org/10.1007/s00024-019-02160-0>
- Moore, J. D., Yu, H., Tang, C. H., Wang, T., Barbot, S., & Peng, D. (2017). Imaging the distribution of transient viscosity after the 2016  $M_w$  7.1 Kumamoto earthquake. *Science*, 356(6334), 163–167. <https://doi.org/10.1126/science.aal3422>
- Moreno, M. S., Bolte, J., Klotz, J., & Melnick, D. (2009). Impact of megathrust geometry on inversion of coseismic slip from geodetic data: Application to the 1960 Chile earthquake. *Geophysical Research Letters*, 36, L16310. <https://doi.org/10.1029/2009GL039276>
- Muto, J., Moore, J. D. P., Barbot, S., Iinuma, T., Ohta, Y., & Iwamori, H. (2019). Coupled afterslip and transient mantle flow after the 2011 Tohoku earthquake. *Science Advances*, 5(9), eaaw1164.
- Nakano, M., Hori, T., Araki, E., Kodaira, S., & Ide, S. (2018). Shallow very-low-frequency earthquakes accompany slow slip events in the Nankai subduction zone. *Nature Communications*, 9(1), 984. <https://doi.org/10.1038/s41467-018-03431-5>
- Nemat-Nasser, S. (2004). *Plasticity. A treatise on finite deformation of heterogeneous inelastic materials*. Cambridge: Cambridge University Press.
- Nemat-Nasser, S., Lori, M., & Datta, S. K. (1996). Micromechanics: Overall Properties of Heterogeneous Materials. *Journal of Applied Mechanics*, 63(2), 561–561. <https://doi.org/10.1115/1.2788912>
- Newman, A. V., Feng, L., Fritz, H. M., Lifton, Z. M., Kalligeris, N., & Wei, Y. (2011). The energetic 2010  $M_w$  7.1 Solomon Islands tsunami earthquake. *Geophysical Journal International*, 186(2), 775–781. <https://doi.org/10.1111/j.1365-246X.2011.05057.x>
- Newman, A. V., Hayes, G., Wei, Y., & Convers, J. (2011). The 25 October 2010 Mentawai tsunami earthquake, from real-time discriminants, finite-fault rupture, and tsunami excitation. *Geophysical Research Letters*, 38, L05302. <https://doi.org/10.1029/2010GL046498>
- Nikkhoo, M., & Walter, T. R. (2015). Triangular dislocation: an analytical, artefact-free solution. *Geophysical Journal International*, 201(2), 1119–1141. <https://doi.org/10.1093/gji/ggv035>
- Nocquet, J. M. (2018). Stochastic static fault slip inversion from geodetic data with non-negativity and bound constraints. *Geophysical Journal International*, 214(1), 366–385. <https://doi.org/10.1093/gji/ggy146>
- Noda, H., & Lapusta, N. (2013). Stable creeping fault segments can become destructive as a result of dynamic weakening. *Nature*, 493(7433), 518–521. <https://doi.org/10.1038/nature11703>
- Noda, H., Lapusta, N., & Kanamori, H. (2013). Comparison of average stress drop measures for ruptures with heterogeneous stress change and implications for earthquake physics. *Geophysical Journal International*, 193(3), 1691–1712. <https://doi.org/10.1093/gji/ggt074>
- Obara, K., & Kato, A. (2016). Connecting slow earthquakes to huge earthquakes. *Science*, 353(6296), 253–258. <https://doi.org/10.1126/science.aaf1512>
- Okada, Y. (1992). Internal deformation due to shear and tensile faults in a half-space. *Bulletin of the Seismological Society of America*, 82(2), 1018–1040.
- Pelayo, A. M., & Wiens, D. A. (1992). Tsunami earthquakes: Slow thrust-faulting events in the accretionary wedge. *Journal of Geophysical Research*, 97(B11), 15,321–15,337. <https://doi.org/10.1029/92JB01305>
- Peng, Z., & Gombert, J. (2010). An integrated perspective of the continuum between earthquakes and slow-slip phenomena. *Nature Geoscience*, 3(9), 599. <https://doi.org/10.1038/ngeo940>
- Poli, P., & Prieto, G. A. (2016). Global rupture parameters for deep and intermediate-depth earthquakes. *Journal of Geophysical Research: Solid Earth*, 121, 8871–8887. <https://doi.org/10.1002/2016JB013521>
- Prieto, G. A., Parker, R. L., Vernon, F. L., Shearer, P. M., Thomson, D. J., Abercrombie, R., & McGarr, A. (2006). Uncertainties in earthquake source spectrum estimation using empirical Green functions. *Geophysical Monograph - American Geophysical Union*, 170, 69. <https://doi.org/10.1029/170GM08>
- Qiu, Q., Hill, E. M., Barbot, S., Hubbard, J., Feng, W., Lindsey, E. O., & Tapponnier, P. (2016). The mechanism of partial rupture of a locked megathrust: The role of fault morphology. *Geology*, 44(10), 875–878. <https://doi.org/10.1130/G38178.1>
- Radiguet, M., Cotton, F., Vergnolle, M., Campillo, M., Walpersdorf, A., Cotte, N., & Kostoglodov, V. (2012). Slow slip events and strain accumulation in the Guerrero gap, Mexico. *Journal of Geophysical Research*, 117, B04305. <https://doi.org/10.1029/2011JB008801>
- Rhie, J., Dreger, D., Bürgmann, R., & Romanowicz, B. (2007). Slip of the 2004 Sumatra-Andaman earthquake from joint inversion of long-period global seismic waveforms and GPS static offsets. *Bulletin of the Seismological Society of America*, 97(1A), S115–S127. <https://doi.org/10.1785/0120050620>
- Robert, B., & Darragh, B. A. (1987). Bolt: A comment on the statistical regression relation between earthquake magnitude and fault rupture length. *Bulletin of the Seismological Society of America*, 77(4), 1479–1484.
- Romanowicz, B. (1992). Strike-slip earthquakes on quasi-vertical transcurrent faults: Inferences for general scaling relations. *Geophysical Research Letters*, 19(5), 481–484. <https://doi.org/10.1029/92GL00265>
- Ruina, A. (1983). Slip instability and state variable friction laws. *Journal of Geophysical Research*, 88, 10,359–10,370. <https://doi.org/10.1029/JB088iB12p10359>

- Salichon, J., Lundgren, P., Delouis, B., & Giardini, D. (2004). Slip history of the 16 October 1999  $M_w$  7.1 Hector Mine earthquake (California) from the inversion of InSAR, GPS, and teleseismic data. *Bulletin of the Seismological Society of America*, *94*(6), 2015–2027. <https://doi.org/10.1785/0120030038>
- Sallarès, V., & Ranero, C. R. (2019). Upper-plate rigidity determines depth-varying rupture behaviour of megathrust earthquakes. *Nature*, *576*(7785), 96–101. <https://doi.org/10.1038/s41586-019-1784-0>
- Salman, R., Hill, E. M., Feng, L., Lindsey, E. O., Mele Veedu, D., Barbot, S., & Natawidjaja, D. H. (2017). Piecemeal Rupture of the Mentawai Patch, Sumatra: The 2008  $M_w$  7.2 North Pagai Earthquake Sequence. *Journal of Geophysical Research: Solid Earth*, *122*, 9404–9419. <https://doi.org/10.1002/2017JB014341>
- Satake, K., Nishimura, Y., Putra, P. S., Gusman, A. R., Sunendar, H., Fujii, Y., & Yulianto, E. (2013). Tsunami source of the 2010 Mentawai, Indonesia earthquake inferred from tsunami field survey and waveform modeling. *Pure and Applied Geophysics*, *170*(9–10), 1567–1582. <https://doi.org/10.1007/s00024-012-0536-y>
- Satake, K., & Tanioka, Y. (1999). Sources of tsunami and tsunamigenic earthquakes in subduction zones. *Pure and Applied Geophysics*, *154*(3–4), 467–483. <https://doi.org/10.1007/s000240050240>
- Sathiakumar, S., Barbot, S. D., & Agram, P. (2017). Extending resolution of fault slip with geodetic networks through optimal network design. *Journal of Geophysical Research: Solid Earth*, *122*, 10,538–10,558. <https://doi.org/10.1029/2019JB018557>
- Sathiakumar, S., Barbot, S., & Hubbard, J. (2020). Earthquake cycles in fault-bend folds. *Journal of Geophysical Research: Solid Earth*, *125*, e2019JB018557. <https://doi.org/10.1029/2019jb018557>
- Schmidt, D. A., & Gao, H. (2010). Source parameters and time-dependent slip distributions of slow slip events on the Cascadia subduction zone from 1998 to 2008. *Journal of Geophysical Research*, *115*, B00A18. <https://doi.org/10.1029/2008JB006045>
- Scholz, C. H. (1998). Earthquakes and friction laws. *Nature*, *391*, 37–42. <https://doi.org/10.1038/34097>
- Scholz, C. H., Aviles, C., & Wesnousky, S. G. (1986). Scaling differences between large interplate and intraplate earthquakes. *Bulletin of the Seismological Society of America*, *76*(1), 65–70.
- Scuderi, M. M., Colletti, C., Viti, C., Tinti, E., & Marone, C. (2017). Evolution of shear fabric in granular fault gouge from stable sliding to stick slip and implications for fault slip mode. *Geology*, *45*(8), 731–734. <https://doi.org/10.1130/G39033.1>
- Segall, P., Rubin, A. M., Bradley, A. M., & Rice, J. R. (2010). Dilatant strengthening as a mechanism for slow slip events. *Journal of Geophysical Research*, *115*, B12305. <https://doi.org/10.1029/2010JB007449>
- Shearer, P. M., Prieto, G. A., & Hauksson, E. (2006). Comprehensive analysis of earthquake source spectra in southern California. *Journal of Geophysical Research*, *111*, B06303. <https://doi.org/10.1029/2005JB003979>
- Shi, Q., Barbot, S., Shibasaki, B., Matsuzawa, T., Wei, S., & Tapponnier, P. (2020). Structural control and system-level behavior of the seismic cycle at the Nankai trough. *Earth, Planets and Space*, *72*(1), 1–31. <https://doi.org/10.1186/s40623-020-1145-0>
- Simons, M. (2002). Coseismic Deformation from the 1999  $M_w$  7.1 Hector Mine, California, Earthquake as Inferred from InSAR and GPS Observations. *Bulletin of the Seismological Society of America*, *92*(4), 1390–1402. <https://doi.org/10.1785/0120000933>
- Simons, M., Minson, S., Sladen, A., Ortega, F., Jiang, J., Owen, S. E., & Webb, F. H. (2012). The 2011 magnitude 9.0 Tohoku-Oki earthquake: Mosaicking the megathrust from seconds to centuries. *Science*, *332*(6036), 1421–1425. <https://doi.org/10.1126/science.1206731>
- Sobolev, S. V., & Muldashev, I. A. (2017). Modeling seismic cycles of great megathrust earthquakes across the scales with focus at postseismic phase. *Geochemistry, Geophysics, Geosystems*, *18*, 4387–4408. <https://doi.org/10.1002/2017GC007230>
- Somerville, P., Irikura, K., Graves, R., Sawada, S., Wald, D., Abrahamson, N., & Kowada, A. (1999). Characterizing crustal earthquake slip models for the prediction of strong ground motion. *Seismological Research Letters*, *70*(1), 59–80. <https://doi.org/10.1785/gssrl.70.1.59>
- Song, S. G., Beroza, G. C., & Segall, P. (2008). A unified source model for the 1906 San Francisco earthquake. *Bulletin of the Seismological Society of America*, *98*(2), 823–831. <https://doi.org/10.1785/0120060402>
- Steblov, G. M., Kogan, M. G., Levin, B. V., Vasilenko, N. F., Prytkov, A. S., & Frolov, D. I. (2008). Spatially linked asperities of the 2006–2007 great Kuril earthquakes revealed by GPS. *Geophysical Research Letters*, *35*, L22306. <https://doi.org/10.1029/2008GL035572>
- Symithe, S. J., Calais, E., Haase, J. S., Freed, A. M., & Douilly, R. (2013). Coseismic slip distribution of the 2010 M 7.0 Haiti earthquake and resulting stress changes on regional faults. *Bulletin of the Seismological Society of America*, *103*(4), 2326–2343. <https://doi.org/10.1785/0120120306>
- Tarantola, A. (2004). Inverse Problem Theory. <https://doi.org/10.1137/1.9780898717921>
- Thomas, M. Y., Avouac, J. P., Gratier, J. P., & Lee, J. C. (2014). Lithological control on the deformation mechanism and the mode of fault slip on the Longitudinal Valley Fault, Taiwan. *Tectonophysics*, *632*(C), 48–63. <https://doi.org/10.1016/j.tecto.2014.05.038>
- Toh, A., Obana, K., & Araki, E. (2018). Distribution of very low frequency earthquakes in the Nankai accretionary prism influenced by a subducting-ridge. *Earth and Planetary Science Letters*, *482*, 342–356. <https://doi.org/10.1016/j.epsl.2017.10.062>
- Toksoz, M., Reilinger, R., Doll, C., Barka, A., & Yalcin, N. (1999). Izmit (Turkey) earthquake of 17 August 1999: First report. *Seismological Research Letters*, *70*(6), 669–679. <https://doi.org/10.1785/gssrl.70.6.669>
- Tomita, F., Kido, M., Ohta, Y., Iinuma, T., & Hino, R. (2017). Along-trench variation in seafloor displacements after the 2011 Tohoku earthquake. *Science Advances*, *3*(7), e1700113. <https://doi.org/10.1126/sciadv.1700113>
- Toro, G. D., Goldsby, D. L., & Tullis, T. E. (2004). Friction falls towards zero in quartz rock as slip velocity approaches seismic rates. *Nature*, *427*, 436–439. <https://doi.org/10.1038/nature02249>
- Toro, G. D., Hirose, T., Nielsen, S., Pennacchioni, G., & Shimamoto, T. (2006). Natural and experimental evidence of melt lubrication of faults during earthquakes. *Science*, *311*(5761), 647–649. <https://doi.org/10.1126/science.1121012>
- Tsang, L. L. H., Hill, E. M., Barbot, S., Qiu, Q., Feng, L., Hermawan, I., & Natawidjaja, D. H. (2016). Afterslip following the 2007  $M_w$  8.4 Bengkulu earthquake in Sumatra loaded the 2010  $M_w$  7.8 Mentawai tsunami earthquake rupture zone. *Journal of Geophysical Research: Solid Earth*, *121*, 9034–9049. <https://doi.org/10.1002/2016JB013432>
- Vallée, M. (2013). Source time function properties indicate a strain drop independent of earthquake depth and magnitude. *Nature Communications*, *4*, 2606.
- Van Dinther, Y., Gerya, T., Dalguer, L., Mai, P. M., Morra, G., & Giardini, D. (2013). The seismic cycle at subduction thrusts: Insights from seismo-thermo-mechanical models. *Journal of Geophysical Research: Solid Earth*, *118*, 6183–6202. <https://doi.org/10.1002/2013JB010380>
- Veedu, D. M., & Barbot, S. (2016). The Parkfield tremors reveal slow and fast ruptures on the same asperity. *Nature*, *535*(7652), 237–240. <https://doi.org/10.1038/nature17190>
- Venkataraman, A., & Kanamori, H. (2004). Observational constraints on the fracture energy of subduction zone earthquakes. *Journal of Geophysical Research*, *109*, B05302. <https://doi.org/10.1029/2003JB002549>
- Viesca, R. C., & Garagash, D. I. (2015). Ubiquitous weakening of faults due to thermal pressurization. *Nature Geoscience*, *8*(11), 875. <https://doi.org/10.1038/ngeo2554>

- Wald, D. J., & Heaton, T. H. (1994). Spatial and temporal distribution of slip for the 1992 Landers, California earthquake. *Bulletin of the Seismological Society of America*, *84*(3), 668–691.
- Wallace, L. M., Araki, E., Saffer, D., Wang, X., Roesner, A., & Kopf, A. (2016). Near-field observations of an offshore  $M_w$  6.0 earthquake from an integrated seafloor and subseafloor monitoring network at the Nankai Trough, southwest Japan. *Journal of Geophysical Research: Solid Earth*, *121*, 8338–8351. <https://doi.org/10.1002/2016JB013417>
- Wallace, L. M., & Eberhart-Phillips, D. (2013). Newly observed, deep slow slip events at the central Hikurangi margin, New Zealand: Implications for downdip variability of slow slip and tremor, and relationship to seismic structure. *Geophysical Research Letters*, *40*, 5393–5398. <https://doi.org/10.1002/2013GL057682>
- Wallace, L. M., Kaneko, Y., Hreinsdóttir, S., Hamling, I., Peng, Z., Bartlow, N., & Fry, B. (2017). Large-scale dynamic triggering of shallow slow slip enhanced by overlying sedimentary wedge. *Nature Geoscience*, *10*(10), 765. <https://doi.org/10.1038/ngeo3021>
- Walsh, J. J., & Watterson, J. (1988). Analysis of the relationship between displacements and dimensions of faults. *Journal of Structural Geology*, *10*(3), 239–247. [https://doi.org/10.1016/0191-8141\(88\)90057-0](https://doi.org/10.1016/0191-8141(88)90057-0)
- Wang, L., & Barbot, S. (2020). Excitation of San Andreas tremors by thermal instabilities below the seismogenic zone. *Science Advances*, *6*(36), eabb2057. <https://doi.org/10.1126/sciadv.abb2057>
- Wang, T., & Jónsson, S. (2015). Improved SAR amplitude image offset measurements for deriving three-dimensional coseismic displacements. *IEEE Journal of Selected Topics in Applied Earth Observations and Remote Sensing*, *8*(7), 3271–3278. <https://doi.org/10.1109/JSTARS.2014.2387865>
- Wang, Y., Lin, Y. N. N., Simons, M., & Tun, S. T. (2014). Shallow rupture of the 2011 Tarlay earthquake ( $M_w$  6.8), Eastern Myanmar. *Bulletin of the Seismological Society of America*, *104*(6), 2904–2914. <https://doi.org/10.1785/0120120364>
- Wang, T., Shi, Q., Nikkhoo, M., Wei, S., Barbot, S., Dreger, D., & Chen, Q. F. (2018). The rise, collapse, and compaction of Mt. Mantap from the 3 September 2017 North Korean nuclear test. *Science*, *361*, eaar7230. <https://doi.org/10.1126/science.aar7230>
- Wang, T., Wei, S., Shi, X., Qiu, Q., Li, L., Peng, D., & Barbot, S. (2018). The 2016 Kaikōura earthquake: Simultaneous rupture of the subduction interface and overlying faults. *Earth and Planetary Science Letters*, *482*, 44–51. <https://doi.org/10.1016/j.epsl.2017.10.056>
- Wang, H., Xu, C., & Ge, L. (2007). Coseismic deformation and slip distribution of the 1997 7.5 Manyi, Tibet, earthquake from InSAR measurements. *Journal of Geodynamics*, *44*(3–5), 200–212. <https://doi.org/10.1016/j.jog.2007.03.003>
- Wang, Z., Zhang, R., Wang, X., & Liu, G. (2018). Retrieving three-dimensional co-seismic deformation of the 2017  $M_w$  7.3 Iraq earthquake by multi-sensor SAR images. *Remote Sensing*, *10*(6), 857.
- Wei, S., Barbot, S., Graves, R., Lienkaemper, J. J., Wang, T., Hudnut, K., & Helmberger, D. (2015). The 2014  $M_w$  6.1 South Napa earthquake: A unilateral rupture with shallow asperity and rapid afterslip. *Seismological Research Letters*, *86*(2A), 344–354. <https://doi.org/10.1785/0220140249>
- Wei, S., Chen, M., Wang, X., Graves, R., Lindsey, E., Wang, T., & Helmberger, D. (2018). The 2015 Gorkha (Nepal) earthquake sequence: I. Source modeling and deterministic 3D ground shaking. *Tectonophysics*, *722*, 447–461. <https://doi.org/10.1016/j.tecto.2017.11.024>
- Wei, S., Graves, R., Helmberger, D., Avouac, J. P., & Jiang, J. (2012). Sources of shaking and flooding during the Tohoku-Oki earthquake: A mixture of rupture styles. *Earth and Planetary Science Letters*, *333–334*, 91–100. <https://doi.org/10.1016/j.epsl.2012.04.006>
- Wei, S., Helmberger, D., & Avouac, J. P. (2013). Modeling the 2012 Wharton basin earthquakes off-Sumatra: Complete lithospheric failure. *Journal of Geophysical Research: Solid Earth*, *118*, 3592–3609. <https://doi.org/10.1002/jgrb.50267>
- Wei, M., Sandwell, D., Fialko, Y., & Bilham, R. (2011). Slip on faults in the Imperial Valley triggered by the 4 April 2010  $M_w$  7.2 El Mayor-Cucapah earthquake revealed by InSAR. *Geophysical Research Letters*, *38*, L01308. <https://doi.org/10.1029/2010GL045235>
- Weiss, J. R., Qiu, Q., Barbot, S., Wright, T. J., Foster, J. H., Saunders, A., et al. (2019). Illuminating subduction zone rheological properties in the wake of a giant earthquake. *Science Advances*, *5*(12), eaax6720. <https://doi.org/10.1126/sciadv.aax6720>
- Wells, D. L., & Coppersmith, K. J. (1994). New empirical relationships among magnitude, rupture length, rupture area, and surface displacement. *Bulletin of the Seismological Society of America*, *84*(4), 975–1002.
- Weston, J., Ferreira, A. M., & Funning, G. J. (2012). Systematic comparisons of earthquake source models determined using InSAR and seismic data. *Tectonophysics*, *532*, 61–81. <https://doi.org/10.1016/j.tecto.2012.02.001>
- Wyss, M. (1979). Estimating maximum expectable magnitude of earthquakes from fault dimensions. *Geology*, *7*(7), 336–340. [https://doi.org/10.1130/0091-7613\(1979\)7<336:EMEMOE>2.0.CO;2](https://doi.org/10.1130/0091-7613(1979)7<336:EMEMOE>2.0.CO;2)
- Yabuki, T., & Matsu'ura, M. (1992). Geodetic data inversion using a Bayesian information criterion for spatial distribution of fault slip. *Geophysical Journal International*, *109*(2), 363–375. <https://doi.org/10.1111/j.1365-246X.1992.tb00102.x>
- Yamazaki, Y., Lay, T., Cheung, K. F., Yue, H., & Kanamori, H. (2011). Modeling near-field tsunami observations to improve finite-fault slip models for the 11 March 2011 Tohoku earthquake. *Geophysical Research Letters*, *38*, L00G15. <https://doi.org/10.1029/2011GL049130>
- Ye, L., Lay, T., Kanamori, H., & Rivera, L. (2016a). Rupture characteristics of major and great ( $M_w \geq 7.0$ ) megathrust earthquakes from 1990 to 2015: 1. Source parameter scaling relationships. *Journal of Geophysical Research: Solid Earth*, *121*, 826–844. <https://doi.org/10.1002/2015JB012426>
- Ye, L., Lay, T., Kanamori, H., & Rivera, L. (2016b). Rupture characteristics of major and great ( $M_w \geq 7.0$ ) megathrust earthquakes from 1990 to 2015: 2. Depth dependence Lingling. *Journal of Geophysical Research: Solid Earth*, *121*, 845–863. <https://doi.org/10.1002/2015JB012426.Rupture>
- Yu, S. B., Kuo, L. C., Hsu, Y. J., Su, H. H., Liu, C. C., & Hou, C. S. (2001). Preseismic deformation and coseismic displacements associated with the 1999 Chi-Chi, Taiwan, earthquake. *Bulletin of the Seismological Society of America*, *91*(5), 995–1012. <https://doi.org/10.1785/0120000722>
- Yue, H., Lay, T., Rivera, L., An, C., Vigny, C., Tong, X., & Báez Soto, J. C. (2014). Localized fault slip to the trench in the 2010 Maule, Chile  $M_w = 8.8$  earthquake from joint inversion of high-rate GPS, teleseismic body waves, InSAR, campaign GPS, and tsunami observations. *Journal of Geophysical Research: Solid Earth*, *119*, 7786–7804. <https://doi.org/10.1002/2014JB011340>
- Yue, H., Lay, T., Schwartz, S. Y., Rivera, L., Protti, M., Dixon, T. H., & Newman, A. V. (2013). The 5 September 2012 Nicoya, Costa Rica  $M_w$  7.6 earthquake rupture process from joint inversion of high-rate GPS, strong-motion, and teleseismic P wave data and its relationship to adjacent plate boundary interface properties. *Journal of Geophysical Research: Solid Earth*, *118*, 5453–5466. <https://doi.org/10.1002/jgrb.50379>
- Zeng, Y., & Anderson, J. G. (2000). Evaluation of numerical procedures for simulating near-fault long-period ground motions using Zeng method. Pacific Earthquake Engineering Research Center.
- Zigone, D., Rivet, D., Radiguet, M., Campillo, M., Voisin, C., & Cotte, N. (2012). Triggering of tremors and slow slip event in Guerrero, Mexico, by the 2010  $M_w$  8.8 Maule, Chile, earthquake. *Journal of Geophysical Research*, *117*, B09304. <https://doi.org/10.1029/2012JB009160>